Peroxomolybdenum Complexes as Epoxidation Catalysts in Biphasic Hydrogen Peroxide Activation: Raman Spectroscopic Studies and Density Functional Calculations

Günter Wahl,[a] Dirk Kleinhenz,[a] Andrea Schorm,[a] Jörg Sundermeyer,*[a] Ralf Stowasser,[b] Christian Rummey,[b] Gerhard Bringmann,*[b] Claudia Fickert,[c] and Wolfgang Kiefer*[c]

Dedicated to Professor Helmut Werner on the occasion of his 65th birthday

Abstract: Density functional calculations and Raman spectroscopic data were correlated with the unique catalytic epoxidation activity of peroxomolybdenum complexes $[MoO(O_2)_2(OER_3)]$ (E = N, P, As; R = *n*-dodecyl) in a biphasic chloroform – 1-octene/aqueous hydrogen peroxide system. Crystal structure determinations on $[MoO(O_2)_2(OPtBu_3)(OCMe_2)]$ and two complexes containing chelating hemilabile ether – phosphane oxide and ether – arsane oxide ligands $[MoO(O_2)_2\{iPr_2E(O)CH_2CH_2OCH_3\}]$ (E = P, As) are reported. A mechanistic study with these model complexes reveals the importance of free coordination sites for peroxide activation. Calculations and Raman spectroscopic data indicate the tendency of coordinatively unsaturated species $[MoO(O_2)_2(L)]$ to dimerize in noncoordinating solvents. The catalytic activity in the presence of water as competing ligand could be correlated with the calculated proton affinity of the ligands OER_3 (R = N, P, As). Elucidation of the vibrational behavior of the structurally characterized peroxo complexes was supported by normal-coordinate analyses.

Keywords: density functional calculations · epoxidation · molybdenum · peroxo complexes · Raman spectroscopy

Introduction

Mimoun-type peroxo complexes $[MO(O_2)_2L_x]$ (M = Mo, W; L = hmpa, dmf, and so on; $x = 1, 2$) have been investigated extensively as stoichiometric reagents for the epoxidation of olefins.[1–3] Attempts to make these neutral molybdenum complexes catalytically active in hydrogen peroxide activation had limited success. The best oxidant system reported to date involves molybdenum and tungsten complexes with alkyl-substituted pyridine *N*-oxides or phosphoric acid amides as ligands in the presence of sulfuric acid as cocatalyst. However, mixtures of epoxide and diol were obtained in only moderate yields even when the oxidant was hydrogen peroxide at up to 100 %.[4] This may have been why the concept of using neutral peroxo complexes for epoxidations with hydrogen peroxide was dropped in favor of the Venturello – Ishii strategy of using heteropolyoxo metalates of molybdenum and tungsten under phase-transfer conditions,[5] which is still the focus of interesting new developments.[6]

To economize on active metal, mononuclear and neutral (and thus electron-poorer) catalysts would be preferable in electrophilic oxidations. A perfect example of metal economy is Herrmann's discovery, the isoelectronically related methylrhenium trioxide (MTO)/hydrogen peroxide oxidant system, which does not tend to oligomerize to polynuclear anionic complex species.[7] However, MTO is expensive compared with molybdenum trioxide, the precursor to Mimoun-type complexes. Other problems are catalyst deactivation by cleavage of the Re–C bond during prolonged use, and inefficient recycling of the catalyst. Our motivation to find suitable process conditions and ligand design for efficient catalytic hydrogen peroxide activation by mononuclear molybdenum and tungsten peroxides was stimulated by the clear structural and isoelectronic relationship between peroxo

[a] Prof. Dr. J. Sundermeyer,[+] Dr. G. Wahl, D. Kleinhenz, A. Schorm
Fachbereich Chemie der Universität Marburg
Hans-Meerweinstrasse, D-35032 Marburg (Germany)
Fax: (+49)6421-28-25693

[b] Prof. Dr. G. Bringmann,[++] Dr. R. Stowasser, C. Rummey
Institut für Organische Chemie der Universität Würzburg
Am Hubland, D-97074 Würzburg (Germany)
Fax: (+49)931-888-4755

[c] Prof. Dr. W. Kiefer,[+++] Dr. C. Fickert
Institut für Physikalische Chemie der Universität Würzburg
Am Hubland, D-97074 Würzburg (Germany)
Fax: (+49)931-888-6332

[+] Catalytic studies

[++] Theoretical studies

[+++] Raman studies

  0947-6539/99/0511-3237 $ 17.50+.50/0

complexes of Group 5–7 metals, for example $[Q]^+[VO(O_2)_2L_2]^-$,[8] $[MO(O_2)_2L_2]$ (M = Cr, Mo, W),[9] and $[ReO(O_2)_2(CH_3)L]$[7] (Figure 1).

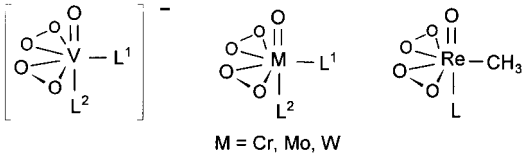

Figure 1. Isoelectronic peroxo complexes of Group 5–7 metals.

The catalytic ability of peroxo complexes of molybdenum can be tuned to activate alkyl hydroperoxides by introducing electron-withdrawing substituents at the chelating pyrazolylpyridine ligand system,[10] but these complexes seem to be poor catalysts in aqueous hydrogen peroxide activation. Here we disclose details of a catalytic biphasic oxidant system, based on neutral molybdenum peroxo complexes $[MoO(O_2)_2L(H_2O)]$, that is the first reported to exhibit a catalytic performance in aqueous hydrogen peroxide activation which is competitive with the homogeneous $[ReO(O_2)_2R(H_2O)]$ system.[11]

Results and Discussion

We found that the ligand L in complexes $[MoO(O_2)_2L(H_2O)]$ has a pronounced impact on their catalytic performance in hydrogen peroxide activation. When L belongs to the extensively studied ligand classes of pyridines, pyridine *N*-oxides, pyrazoles, $OPPh_3$, DMF, HMPA, or derivatives thereof, the complexes show poor activity in epoxidations. The activity is even lower if L is a strongly bonded chelating ligand or if the coordinated water is substituted by a second ligand L. However, we observed a dramatic increase in activity if the ligand L was a long-chain trialkylamine oxide, trialkylphosphane oxide or trialkylarsane oxide. The greatest ligand acceleration compared with the catalytically inactive bis(aqua) complexes is observed when exactly one coordinated water molecule in $[MoO(O_2)_2(H_2O)_2]$ is replaced by an arsane oxide with three *n*-alkyl chains, preferably longer than C_{10}.

Catalytic studies: The catalysts are easily prepared from solutions of peroxomolybdic acid $[MoO(O_2)_2(H_2O)_2]$ in aqueous hydrogen peroxide, which are formed upon dissolving MoO_3 in aqueous 10–30% hydrogen peroxide at pH 2–4.[1] In the hydrophilic environment of the aqueous phase the bis(aqua) complex is catalytically inactive in epoxidation reactions, as are complexes $[MoO(O_2)_2(H_2O)L]$ (L = OE*n*Bu$_3$, E = N, P, As, hmpt), which are formed when the short-chain Group 5 element oxides are added in THF.[1, 2a] In contrast, addition of tris(*n*-dodecyl)amine oxides, phosphane oxides, or arsane oxides in a solvent immiscible with water, preferably chloroform, leads to a highly active catalytic system, which involves the formation of catalysts $[MoO(O_2)_2(OEnDodec_3)]$ (E = N, P, As).

The free ligands OE*n*Dodec$_3$ are white solids that are insoluble in water but soluble in hydrocarbons, whereas the aqueous peroxomolybdic acid is completely insoluble in chloroform. It is plausible that at the interface of the organic and aqueous phases the better-coordinating Group 5 trialkyl–element oxide donors substitute water as a ligand, thus extracting the inorganic peroxide into the organic phase. The extraction of the yellow peroxomolybdic acid can be observed through the fading of the yellow color of the aqueous phase while the yellow color of the organic phase increases when the biphasic system is stirred. Scheme 1 depicts the biphasic reaction medium.

To estimate the rate-limiting factors of this catalytic process is a very complex problem, because many parameters have a strong influence on the overall catalytic performance. The most important parameter is probably the concentration of the catalytically active species in the organic phase, where the

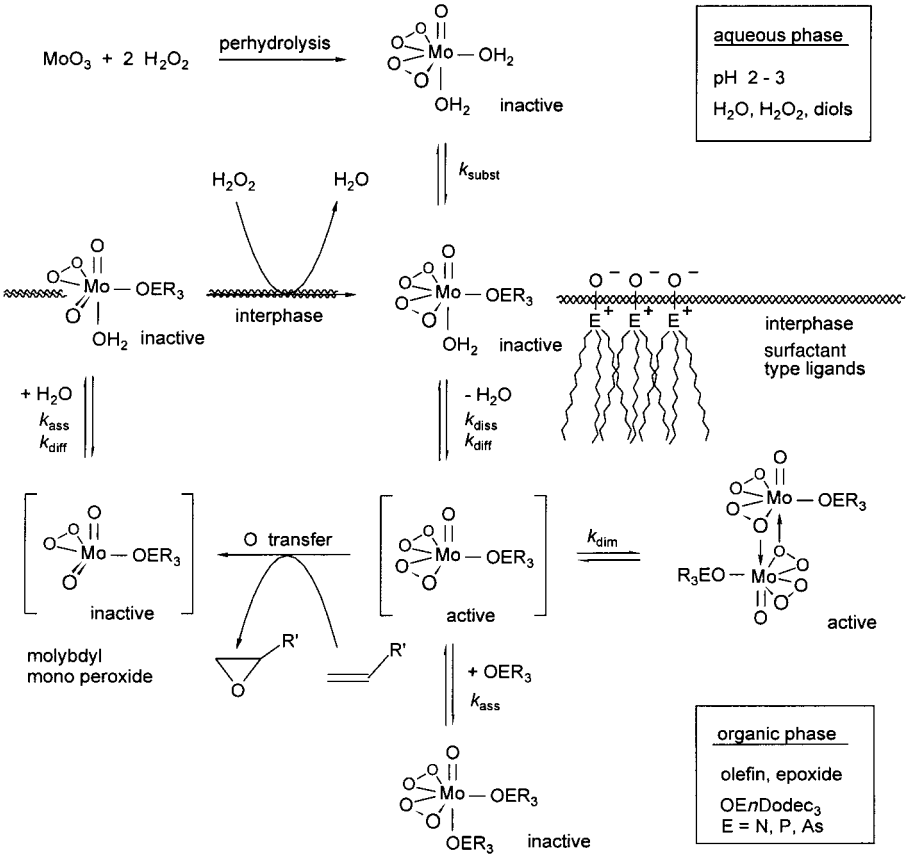

Scheme 1. Schematic view of the biphasic oxidation system applying non-ionic, surfactant-type ligands as phase-transfer agents.

0947-6539/99/0511-3238 $ 17.50+.50/0 *Chem. Eur. J.* **1999**, *5*, No. 11

O-transfer step takes place. This concentration is dependent on the lipophilicity of L. We find, for example, that the amine oxide ON*n*Dodec$_3$ is a better-extracting ligand than the commercial surfactant ONMe$_2$(stearyl). The nature of the ligand L = OE*n*Dodec$_3$ (E = N, P, As) seems to have similar importance. Its affinity for the metal Lewis acid compared with the competing aqua ligand determines how much of the active species is extracted into the organic phase. We find that in their extraction ability arsane oxides are superior to amine oxides, which are highly superior to phosphane oxides of the same alkyl chain length. The concentration of the active species [MoO(O$_2$)$_2$(OE*n*Dodec$_3$)] in the organic phase also depends on the equilibrium constants of reactions such as the binding of a second ligand L (deactivating, L = OE*n*Dodec$_3$ or water; or activating, L = H$_2$O$_2$). Our mechanistic studies described below reveal that the best catalytic performance is observed when the coordination of even only one monodentate Group 5 element oxide ligand leads to quantitative extraction of the peroxomolybdic acid into the organic phase. The other coordination site at the more labile axial position *trans* to the oxo functionality is probably required for the coordination and activation of hydrogen peroxide to give an even more reactive oxenoid than the bis(peroxo) complex (see below).

The overall reaction rate also depends on the rates of four individual steps: the rate of oxygen transfer, the rate of diffusion to the interphase, the rate of perhydrolysis regenerating the catalytically active species, and the rate of dissociation into the active species and water. Finally it depends on the rate of diffusion back into the organic phase. Our stoichiometric epoxidation experiments (see below) show that the rate of O transfer is determined by the electrophilicity of the oxenoid[12] which is extracted into the organic phase. In this respect the situation becomes complex because the better-extracting ligand L (with the higher donor strength) will at the same time reduce the electrophilicity (O-transfer ability) of the oxenoid to a greater extent. Similarly the better donor quality of an oxo ligand compared with a peroxo ligand may be the reason why the active bis(peroxo) species may transfer only one oxygen atom and not two. The metal species remaining after oxygen transfer (a conceivable intermediate would be the molybdyl monoperoxide [MoO$_2$(O$_2$)(OE*n*Dodec$_3$)(H$_2$O)$_n$]) seems to lack sufficient electrophilicity at the remaining peroxo group to transfer the other oxygen to the olefinic substrate. The rate of regenerating the catalytically active species is dependent on the rate of diffusion to the interphase and the rate of perhydrolysis of one of its [M=O] functionalities in contact with aqueous hydrogen peroxide. Therefore the variation of such parameters as stirring speed and reactor design (diffusion control versus reaction control), the pH[13] of the aqueous hydrogen peroxide, and the identity of the water-immiscible organic solvent and the central atom (molybdenum or tungsten) have an influence on the turnover frequency (TOF) of the catalytic process.[14] Facing such a complex situation, we have evaluated only three complexes under identical conditions in the epoxidation of cyclooctene and 1-octene using magnetically stirred reaction tubes. The results are summarized in Table 1.

With our catalytic system even nonactivated α-olefins such as 1-octene, which are known to be oxidized 100–1000 times more slowly than cycloolefins, are converted with high selectivities to the corresponding epoxides. In experiments 1–3 a 1-octene/30% H$_2$O$_2$/catalyst mixture (molar proportions 1/4/0.04) was chosen to achieve high conversions of the olefin. In these experiments, which resembled typical laboratory preparations, the epoxide yields based on converted olefin (epoxide selectivities) were above 90%. However, due to unproductive decay of excess hydrogen peroxide in the presence of the active oxenoid, the yields of epoxide based on hydrogen peroxide consumed (hydrogen peroxide selectivities) were found to be much lower. The hydrogen peroxide content before and after epoxidation was determined cerimetrically to provide a measure of the productive O transfer from the oxidant. This shows clearly that conversions approach a limit mainly due to decay of hydrogen peroxide and not to decay of the very robust catalyst (at least for OPR$_3$ and OAsR$_3$ ligands). For preparative laboratory procedures addition of 3–5 equiv hydrogen peroxide in small portions is more desirable if high conversions of α-olefins as well as high yields of isolated epoxide yields are required (see Experimental Section).

Much better yields of epoxide, based on hydrogen peroxide consumed as well as on olefin consumed, can be obtained by using excess olefin relative to hydrogen peroxide (experiments 4–6, 7–9). Therefore lower concentrations of the

Table 1. Catalytic epoxidation of 1-octene (entries 1–6) and cyclooctene (entries 7–9) with H$_2$O$_2$ and [MoO$_3$L(H$_2$O)] as catalyst under biphasic conditions CHCl$_3$/30% H$_2$O$_2$ (60 °C).[a]

Entry	Catalyst[b] [MoO$_3$L(H$_2$O)] L	Molar ratio olefin:H$_2$O$_2$:cat	Reaction time [h]	Olefin conversion [%]	Epoxide yield[c] [%]	Epoxide yield[d] [%]
1	ON*n*Dodec$_3$	1:4:0.04	24	75	95	19
2	OP*n*Dodec$_3$	1:4:0.04	24	14	93	11
3	OAs*n*Dodec$_3$	1:4:0.04	24	83	96	25
4	ON*n*Dodec$_3$	4:1:0.01	24	8	> 98	53
5	OP*n*Dodec$_3$	4:1:0.01	24	1	> 98	67
6	OAs*n*Dodec$_3$	4:1:0.01	24	24	> 98	92
7	ON*n*Dodec$_3$	4:1:0.005	2	25	99	92
8	OP*n*Dodec$_3$	4:1:0.005	2	1	99	93
9	OAs*n*Dodec$_3$	4:1:0.005	2	25	> 99	> 99

[a] Conversions and selectivities were determined by quantitative GC with di-*n*-butyl ether as internal standard. [b] Catalysts were formed in situ by adding one equivalent of the ligand L in CHCl$_3$ to a solution of [MoO$_5$(H$_2$O)$_2$] in 30% hydrogen peroxide (pH 2.6 ± 0.2). [c] Based on consumed olefin. [d] Based on consumed hydrogen peroxide.

catalyst and olefin/30% H_2O_2 in an inverse molar ratio (4:1) were employed to measure the selectivity of productive O transfer from hydrogen peroxide, which is 100% when the selective olefin conversion approaches 25%. Under these conditions there is always enough olefin present to quench the active oxenoid before (in the presence of hydrogen peroxide) it is decomposed unproductively to oxygen and water. As expected, cyclooctene (experiments 7–9) is much more readily oxidized than 1-octene (experiments 4–6). Epoxide yields based on olefin consumed exceeded 98%, as ring opening to diols was suppressed efficiently under these biphasic conditions. A high concentration of cyclooctene (the best quencher for the active oxenoid; experiments 7–9) or of 1-octene (experiment 6) guarantees high yields even of epoxides (>90%) based on hydrogen peroxide consumed. For cyclooctene, TONs exceeding 200 and turnover frequencies (TOFs) of $100\,h^{-1}$ are obtained (experiments 7, 9).

Our procedure has many advantages. The olefin is epoxidized in the organic phase and the epoxide is kept separate from the highly acidic aqueous phase. Thus the acid-catalyzed ring opening of the epoxides to the synthetically less desirable diols is suppressed efficiently and the epoxides can be recovered easily from the organic phase (for instance by distillation or flash chromatography). The concentration of the active oxenoid in the organic phase is almost independent of the hydrogen peroxide concentration, which may range from 5 to 50%. This observation could be interpreted in terms of the rate of perhydrolysis at the interphase being high, even at low hydrogen peroxide concentrations, while the O-transfer step in the organic phase is rate determining. The extraction of the active oxenoid is an important advantage since water, which is formed as a by-product, is continuously diluting the oxidant.

Preparation of catalysts and their model complexes: To prove that the catalysts are Mimoun-type mononuclear complexes we endeavored to isolate and characterize dodecyl derivatives $[MoO(O_2)_2(OER_3)(H_2O)]$. However, only complexes $[MoO(O_2)_2(OER_3)]$ (E = N (**1**), P (**2**), As (**3**); R = *n*-dodecyl) without any coordinated aqua ligand were isolated after the solvent was stripped at room temperature and reduced pressure. Elemental analyses, and IR, Raman, and proton NMR spectra gave no indication of the presence of any water molecule within the highly hydrophobic coordination sphere, so the question arose of how such coordinatively unsaturated species might be stabilized in aprotic media. In accord with the assumption that they would show a tendency to dimerize (Scheme 2), the molecular weight of **2** in cyclohexane determined cryoscopically was 1397; the calculated molecular weight of the dimer of **2** is 1461.8.

Tris(*tert*-butyl)phosphane oxide was used to increase the solubility and to test whether the steric demand of the ligands had any effect on the catalytic activity of the dehydrated model complex $[MoO(O_2)_2(OPtBu_3)]$.[15] We found, however, that only an increase in the solubility of the complex in organic solvents, but not an increase in the phosphane oxide cone angle, had any catalytic acceleration effect. Complexes of the commercially available surfactant $OPnOct_3$ have proven to be more active than $OPtBu_3$ derivatives. Although we were not able to isolate a bis(phosphane) adduct with $OPtBu_3$, its steric demands could not prevent smaller ligands such as water or acetone from tending to coordinate. From an acetone-containing solution single crystals of $[Mo(O)(O_2)_2(OPtBu_3)(OCMe_2)]$ (**4**) were grown. The acetone is weakly bonded and is readily lost in vacuo at room temperature.

For a mechanistic study we designed two model complexes **5** and **6** with a new chelating hemilabile ether–phosphane oxide or ether–arsane oxide ligand system. These complexes are formed in good yields when the respective ligands $iPr_2E(O)CH_2CH_2OMe$ (E = P, As) are added to solutions of peroxomolybdic acid. It was expected that the weakly coordinating ether chelate would allow investigation of the reactions of these soluble model complexes under absolute aprotic conditions. The ether oxygen atom occupies a coordination site that under catalytic conditions is occupied by water, hydrogen peroxide, or the oxygen atom of a bridging η^2-peroxo group in a dinuclear species (Scheme 2).

Furthermore, a peroxo complex **7** containing two *n*-dodecylphosphane oxide ligands was isolated and characterized to discover whether catalysts with two long-chain element oxide ligands may be generated under catalytic conditions and whether there may be a catalytic inhibition effect when all the coordination sites at molybdenum are occupied by strong donors. The existence of **7** was proven unambiguously by its elemental analysis and its dynamic

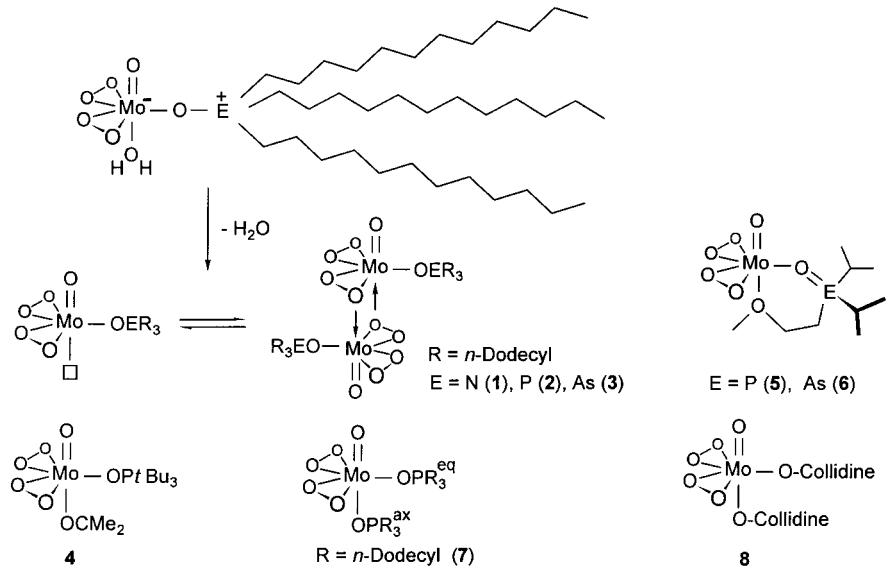

Scheme 2. Catalysts **1**–**3** and model complexes **4**–**8**.

0947-6539/99/0511-3240 $ 17.50+.50/0 *Chem. Eur. J.* **1999**, *5*, No. 11

behavior observed in a variable-temperature ^{31}P NMR experiment. At room temperature two resonances, $\delta(^{31}P) = 77.4$ and 57.4, are observed, with the free ligand at $\delta(^{31}P) = 44.3$. We assign the more deshielded resonance to the more strongly bonded equatorial phosphane oxide, and the less deshielded resonance to the more weakly bonded axial phosphane oxide. When the temperature is raised the signals broaden, and coalescence is observed at $\delta(^{31}P) = 66.5$ ($T_C = 363$ K, 81.0 MHz). From this NMR experiment, for the first time to the best of our knowledge, it is possible to estimate the Gibbs energy of dynamic ligand exchange in pseudo trigonal-bipyramidal Mimoun-type peroxo species: $\Delta G^{\neq}$ ($T_C = 363$ K) $= 87.0 \pm 0.3$ kJ mol^{-1}. This dynamic ligand exchange with or without M–L bond cleavage (Berry pseudo-rotation) has to be considered if stereorigid chiral ligands for asymmetric catalysis are incorporated in this type of peroxo complex.

We selected the collidine *N*-oxide complex **8** for our set of catalyst models. The bis-adduct **8** is precipitated from a solution of peroxomolybdic acid, even when collidine *N*-oxide is added in substoichiometric amounts (L/M < 1). The coordinatively saturated complex **8** is a very poor oxidant in stoichiometric epoxidations and it is catalytically inactive in the hydrogen peroxide activation.

Crystal structures of model complexes: Single crystals of the three model peroxides **4**–**6** were obtained by cooling saturated solutions in chloroform/acetone. Their crystal structures and selected bond lengths and angles are shown in Figures 2–4.

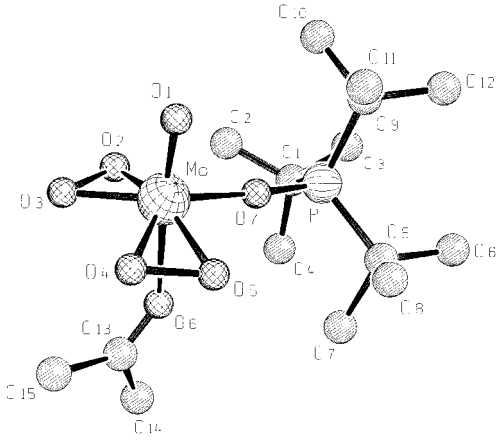

Figure 2. Molecular structure of **4** (H atoms omitted for clarity). Selected bond lengths [pm] and angles [°]: Mo–O1 166.8(4), Mo–O2 193.6(4), Mo–O3 192.0(4), Mo–O4 191.8(4), Mo–O5 193.0(4), Mo–O6 244.8(4), Mo–O7 203.0(4), O2–O3 147.5(6), O4–O5 146.6(6), P–O7 151.9(4), P–C1 187.4(6), P–C4 186.6(6), P–C7 188.2(6), O6–C13 121.5(7), O1-Mo-O2 102.8(2), O1-Mo-O3 102.4(2), O1-Mo-O4 102.1(2), O1-Mo-O5 103.5(2), O2-Mo-O3 45.0(2), O4-Mo-O5 44.8(2), O2-Mo-O7 87.5(2), O5-Mo-O7 86.9(2), O1-Mo-O6 173.2(2), O1-Mo-O7 96.8(2), O6-Mo-O7 76.48(13), Mo-O7-P 175.7(2), Mo-O6-C13 138.6(4).

The three molecular structures reveal the characteristic distorted trigonal-bipyramidal coordination geometry if the two η^2-peroxo groups coplanar with the equatorial plane are considered to occupy one coordination site. The metal center is located slightly above the equatorial plane defined by the

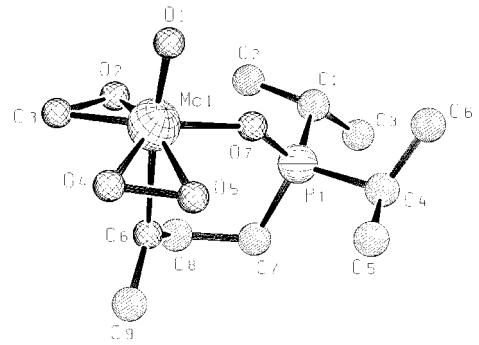

Figure 3. Molecular structure of **5** (H atoms omitted for clarity). Selected bond lengths [pm] and angles [°]: Mo–O7 204.9(2), Mo–O6 242.4(2), Mo–O1 167.2(2), Mo–O4 192.1(2), Mo–O2 193.3(2), Mo–O5 194.1(2), Mo–O3 192.1(2), O2–O3 147.5(2), O4–O5 147.3(3), P–O7 152.7(2), P–C4 180.7(3), P–C1 180.9(2), P–C7 180.9(3), O6–C8 142.3(3), O6–C9 143.2(3), O6-Mo-O7 78.15(6), O1-Mo-O7 94.36(8), O1-Mo-O3 102.68(9), O1-Mo-O2 102.72(10), O1-Mo-O5 101.91(10), O1-Mo-O4 102.25(10), O1-Mo-O6 172.48(8), O2-Mo-O3 45.01(7), O4-Mo-O5 44.84(8), O2-Mo-O7 87.07(7), O7-Mo-O5 88.63(7), O2-Mo-O6 76.44(7), O6-Mo-O5 78.82(8), O7-P-C7 111.10(11), O7-P-C4 108.74(10), O7-P-C1 108.21(10), Mo-O6-C8 121.31(14), P-O7-Mo 146.45(9).

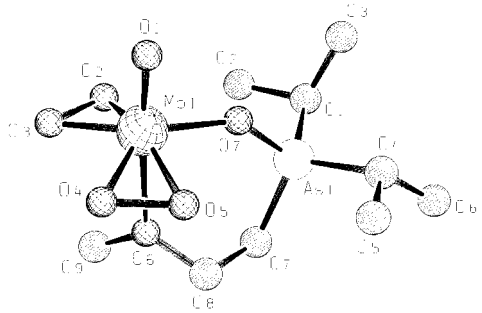

Figure 4. Molecular structure of **6** (H atoms omitted for clarity). Selected bond lengths [pm] and angles [°]: Mo–O7 199.0(5), Mo–O6 244.9(5), Mo–O1 165.8(5), Mo–O2 193.5(5), Mo–O5 192.9(5), Mo–O4 193.5(5), Mo–O3 191.2(6), O4–O5 147.0(8), O2–O3 144.0(8), As–O7 170.3(5), As–C1 193.2(8), As–C4 191.6(8), As–C7 194.3(7), O6–C9 142.8(9), O6–C8 142.8(10), O7-Mo-O6 79.9(2), O1-Mo-O7 95.5(2), O3-Mo-O1 102.0(3), O5-Mo-O1 102.7(3), O1-Mo-O2 102.6(3), O1-Mo-O3 101.7(3), O1-Mo-O6 175.4(2), O4-Mo-O5 44.7(2), O2-Mo-O3 44.0(2), O7-Mo-O5 87.3(2), O7-Mo-O2 88.9(2), O5-Mo-O6 76.7(2), O2-Mo-O6 77.9(2), O7-As-C7 109.8(3), O7-As-C1 106.4(3), O7-As-C4 106.7(3), Mo-O6-C8 123.9(5), As-O7-Mo 143.7(3).

five oxygen atoms, which is typical for this structural class.[16–19] The Mo–O bond lengths and angles within the $[Mo(O)(O_2)_2]$ fragments seem to be only slightly influenced by the donor strength and steric demands of the neutral ligands attached to this structural moiety. In all three structures we find the most weakly bonded ligand with the longest Mo–O distance in an axial position *trans* to the oxo ligand. The oxo ligand is the stongest π-donor within the ligand regime, thus showing the strongest *trans* influence. The weaker π-donor ligands $[O_2]^{2-}$ and OER_3 are *cis*, and the weakest donor is *trans*, to the oxo ligand. The bond lengths and angles within the peroxo groups are not influenced significantly by the coligands. A selection of more deviant structural features is shown in Table 2. The differences in the Mo–O bond lengths of the oxo ligand should have an impact on the vibrational behavior of these compounds. The Mo–O7 distances reveal that the arsane oxide is more strongly bonded

Table 2. Comparison of selected bond lengths [pm] and angles [°] in the molecular structures of **4**, **5**, and **6.**

Structural feature	$OPtBu_3/OCMe_2$ **4** (E = P)	$iPr_2P(O)CH_2CH_2OCH_3$ **5** (E = P)	$iPr_2As(O)CH_2CH_2OCH_3$ **6** (E = As)
Mo–O(1)	166.8(4)	167.2(2)	165.8(5)
Mo–O(7)	203.0(4)	204.9(2)	199.0(5)
Mo–O(6)	244.8(4)	242.4(2)	244.9(5)
E–O(7)	151.9(4)	152.7(2)	170.3(5)
E-O(7)-Mo	175.7(2)	146.45(9)	143.7(3)

to the metal center than the two phosphane oxide ligands. This can be explained by the short E–O7 distance in the phosphane oxide, which allows a much better stabilization of the negative charge at oxygen by negative hyperconjugation than in the arsane oxide. As a consequence of the better donor capability of the arsane oxide, the corresponding ether donor is more weakly bonded than in the hemilabile ether–phosphane oxide. The π-donor capability of a monodentate phosphane oxide may also be seen in the nearly linear bonding (Mo-O7-P 175.7(2)° in **4**). The bond angles Mo-O7-E within the corresponding constrained-geometry chelate structures **5** and **6** are the largest found so far for six-membered ring structures of this type.[16]

Mechanistic studies: Stoichiometric epoxidation experiments were carried out to gain insight into the nature of the active oxenoid and to demonstrate the effect of catalyst inhibition by strongly chelating ligands or even by two strongly nonchelating donors. The yields of epoxide after 16 h of reaction at 60 °C of coordinatively unsaturated complex **1** with equimolar amounts of 1-octene (Figure 5, run B) were determined, and

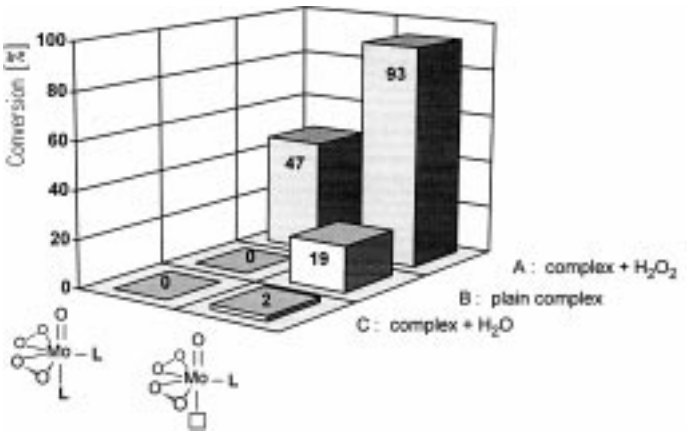

Figure 5. Stoichiometric epoxidation of 1-octene by 1 equiv **1** or $[MoO(O_2)_2(ONnDodec_3)_2]$; conversion after 16 h, 60 °C, $CHCl_3$.

also after addition of 8 equiv water (run C) or 4 equiv aqueous 30% hydrogen peroxide (run A). A similar series of three runs was monitored in the presence of 2 equiv ligand $ONndodec_3$ per mol molybdenum (Figure 5).

In general the O-transfer ability of mono(amine oxide) complexes is higher that that of bis(amine oxide) adducts. The O transfer is strongly inhibited in the presence of water or of a second amine oxide blocking the reactive coordination site (runs C and B). However, an oxenoid more reactive than an $[M(\eta^2\text{-}O_2)]$ function was generated in the presence of 30% hydrogen peroxide (4 equiv). Under these conditions even the bis(amine oxide) complex yielded 47% epoxide, compared with 93% for the mono-substituted complex. Therefore it is conceivable that hydrogen peroxide is converted by reaction with either an oxo function (cycle A, Scheme 3) or a peroxo function (cycle B) into a highly reactive oxenoid.

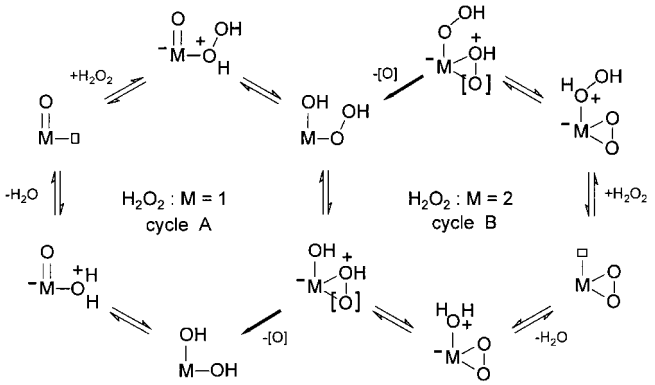

Scheme 3. Plausible intermediates of the perhydrolysis of an oxo function (cycle A) and of a peroxo function (cycle B).

The most reactive oxenoids are expected to be metal peracids that contain an $[M(\eta^2\text{-}OOH)]$ functionality. Protonation of an η^2-peroxo functionality should minimize the barrier of irreversible [O] transfer (where [O] is most reactive site in the oxenoid), as the O–O bond is already polarized (its LUMO should be lower in energy) for a nucleophilic attack of the olefin HOMO at the [O] atom to be transferred. Similar observations have been discussed by Thiel et al. for the activation of alkyl hydroperoxides with peroxo complexes.[16, 19] However, even a η^2-peroxo function may act as an oxenoid, but at a lower rate than any $[M(\eta^2\text{-}OOE)]$ (E = H, $SiMe_3$, CMe_3, d^0-[M] and suchlike) functionality. This is clearly demonstrated in a stoichiometric epoxidation experiment under strictly aprotic conditions with our hemilabile ether–oxide complexes **5** and **6** (Figure 6).

Both complexes transferred only one [O] atom to cyclooctene, so 1 equiv of the olefin remained unreacted. It is interesting that under homogeneous conditions (in the absence of water) the phosphane oxide complex approaches the limit of about 50% epoxide formation much faster than the corresponding arsane oxide. This is probably due to the more electrophilic character of the oxenoid **5** with the weaker donor ligand phosphane oxide. The plausible intermediate molybdyl peroxide has never yet been observed or isolated; we are continuing our efforts to characterize this species, which is not able to transfer any oxygen to olefins. A similar trend in the nonreactivity of plausible mono(peroxo) species was observed for isoelectronically related alkylrhenium catalysts[7] as well as for anionic dinuclear peroxomolyb-

  0947-6539/99/0511-3242 $ 17.50+.50/0 *Chem. Eur. J.* **1999**, *5*, No. 11

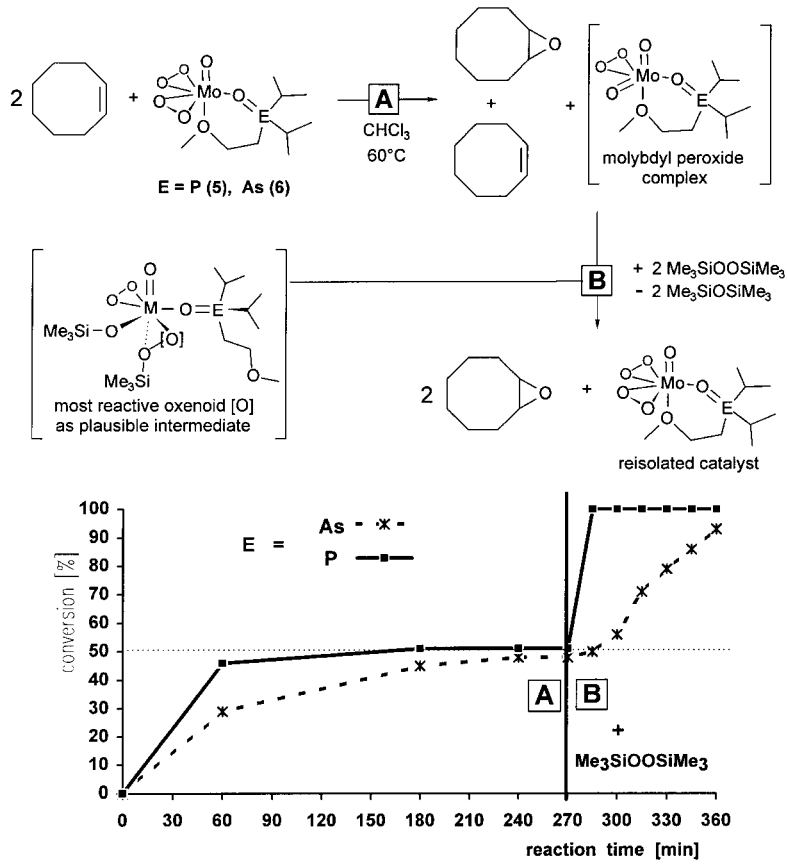

Figure 6. Stoichiometric epoxidation of cyclooctene with **5** and **6** without added $Me_3SiOOSiMe_3$ and after addition of $Me_3SiOOSiMe_3$ at $t = 270$ min.

dates.[26, 27] After 270 min, 2 equiv bis(trimethylsilyl) peroxide, which can be regarded as a nonprotic substitute for 100% H_2O_2, was added. An enormous acceleration in the epoxidation was observed, similar to that described above. After 15 min the conversion was complete in the case of the phosphane oxide complex. We conclude that again an oxenoid that is much more reactive than a η^2-peroxo function is formed by its reaction with hydroperoxides or silyl peroxides. Furthermore this experiment clearly demonstrates that it is only the better extracting ability of more basic arsane oxides in the phase-transfer step of the biphasic catalysis that makes these ligands superior to the less basic phosphane oxides. Under homogeneous aprotic conditions, however, the weaker donors OPR_3 generate the more electrophilic, and thus more active, oxenoids.

Which is the best ligand for catalysis? The commercially available tris(dodecyl)amine (Merck) is the preferred ligand precursor when epoxides have to be prepared on a laboratory scale. As expected, when the amine is added to hydrogen peroxide containing the catalyst it is converted in situ to the amine oxide. For small-scale preparations a catalyst/olefin/H_2O_2 molar ratio of 4:100:400 (Table 1) may be employed. In such experiments epoxides are produced in good yields from cycloolefins and α-olefins. Typical preparations of 1-octene oxide and cyclooctene oxide from cheap, commercially available catalyst precursors are described in the Experimental Section. Tris(*n*-dodecyl)amine *N*-oxide is quite stable under reaction conditions below 60 °C but eventually decomposes at higher temperatures: Bis(*n*-dodecyl)amine and undecanal have been identified by GC/MS among the decomposition products. Therefore, if long catalyst lifetimes (high TONs) and high yields based on hydrogen peroxide are desired, then the arsane oxides are the ligands of choice. An inverse olefin/oxidant molar ratio as well as lower concentrations of the catalyst (for example, catalyst/olefin/$H_2O_2 = 0.5:400:100$) may be employed because arsane oxide complexes have a higher catalyst lifetime and a lower trend toward unproductive hydrogen peroxide decomposition than their amine oxide counterparts. The stoichiometric experiment in homogeneous solution reveals that phosphane oxides are the ligands of choice in a homogeneous nonaqueous solution. Due to their poorer donor strength, phosphane oxides generate more electrophilic oxenoids. However, in a two-phase system they are not sufficiently competitive against the aqua ligand in their extracting ability. Therefore long-chain amine oxides, and especially arsane oxides, are the best ligands in this combination of phase-transfer and O-transfer catalysis. Phosphane oxides are not the preferred ligands as too much of the peroxomolybdic acid remains in the aqueous phase.

Raman spectroscopy: Since no crystal structure determinations have been available for coordinatively unsaturated neutral species $[MoO(O_2)_2(OER_3)]$,[20] we present a combined study of Raman spectroscopic data of coordinatively saturated $[MoO(O_2)_2LL']$ and unsaturated complexes "$[MoO(O_2)_2L]$", a normal-coordinate analysis and density functional (DF) calculations based on structurally characterized precursor complexes, to elucidate the influence of the ligands L or L′ on the bonding between the d^0-metal center and the different oxygen donors. The metal–oxo stretching contributes a strong signal to the IR and Raman spectra between 900 and 1100 cm^{-1} depending on the (Mo–O) bond order.[21, 22] Griffith et al. observed the (O–O) stretching in comparable complexes at approximately 880 cm^{-1} and the metal peroxido stretchings between 500 and 600 cm^{-1}.[23, 24] A simplified normal-coordinate analysis of the central molecular fragment $[MoO(O_2)_2LL']$ was carried out for a detailed vibrational analysis. Furthermore Raman studies on the coordinatively unsaturated complex fragments "$[MO(O_2)_2L]$" were used for structural characterization of plausible dimers of these species.

Group theory: Complexes of the type $[MoO(O_2)_2LL']$ possess C_s symmetry. All vibrations are therefore Raman- and infrared-active. Griffith et al.[23, 24] discussed the vibrations of the metal peroxide triangle under local C_{2v} symmetry, which leads to a type A_1 ν(OO) mode at 880 cm^{-1} and two $\nu(M(O_2))$ modes, types A_1 (symmetric) and B_2 (antisymmetric), between 500 and 600 cm^{-1}. For bis(peroxo) complexes with local C_s symmetry the vibrations of both $[M(O_2)]$ units should be coupled,[2a] leading to a splitting of the three modes into a symmetric (A′) and an antisymmetric (A″) mode (Figure 7).

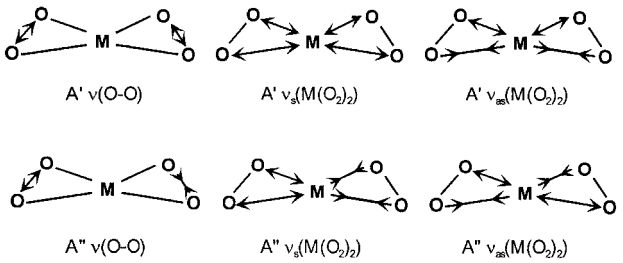

Figure 7. Vibrational modes for bis(peroxo) complexes.

Characteristic vibrational bands: Earlier studies of comparable bis(peroxo) complexes have revealed two signals in the ν(O–O) region of the IR spectra, in contrast to the Raman spectra, which often exhibit only one strong ν(O–O) band at 880 cm^{-1}.[2a, 23, 24] All the Raman spectra of the various molybdenum complexes $[MoO(O_2)_2LL']$ (Figure 8) are dominated by the strong molybdenum–oxo stretching mode at approximately 950 cm^{-1} and the different modes of the bis(peroxo) unit. Beside the strong ν(O–O) band at around 880 cm^{-1} in spectra A and D–F, a weaker signal could be observed with a shift of about -10 cm^{-1}, in accordance with the IR spectra. By means of polarized Raman measurements of $[MoO(O_2)_2(OPtBu_3)(OCMe_2)]$ in $OCMe_2$ and $[MoO(O_2)_2$-$(hmpa)(OH_2)]$ in aqueous solution, the strong signal in this region could be identified as the A′ ν(O–O) mode.

The $\nu(M(O_2)_2)$ modes are located between 500 and 600 cm^{-1}. All the Raman spectra in Figure 8 show one strong signal at approximately 540 cm^{-1}, a medium one around 585 cm^{-1}, and several weaker bands. The two stronger signals are polarized in the Raman spectra of the solution and could be assigned to A′ $\nu(M(O_2)_2)$ modes. The two A″ modes probably possess weaker Raman intensities and could be obscured by the strong A′ vibrational bands or Raman signals of the different ligands L. Figure 9A shows the Raman spectrum of $[MoO(O_2)_2(OPtBu_3)(OCMe_2)]$ between 470 and 620 cm^{-1}, and Figure 9B a band-shape analysis, in which six signals could be separated: two modes of the $OPtBu_3$ ligand occur at 500 and 556 cm^{-1}, so the signals at 526 and 542 cm^{-1} could be assigned to the A″ $\nu(M(O_2)_2)$ modes.

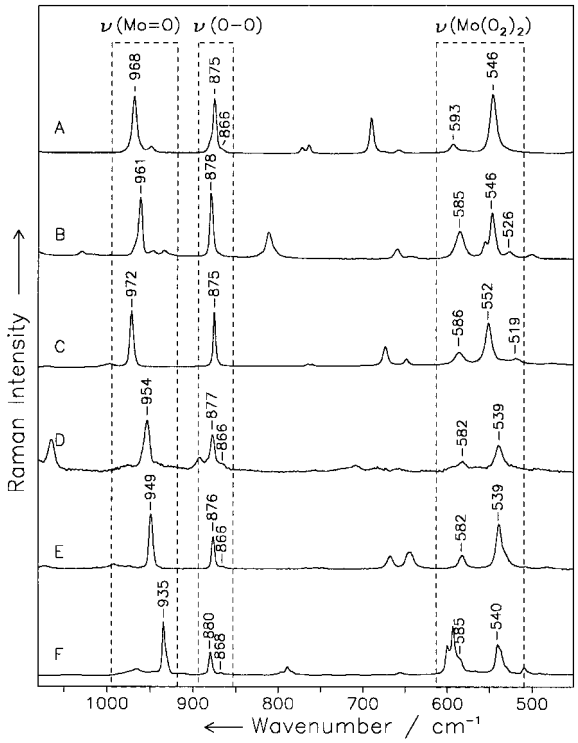

Figure 8. Raman spectra of polycrystalline $[MoO(O_2)_2LL']$. A: L = $OPMe_3$, L′ = OH_2; B: L = $OPtBu_3$, L′ = $OCMe_2$; C: L = hmpa, L′ = OH_2; D: L = L′ = $OPnDodec_3$; E: L = L′ = HMPA; F: L = L′ = ON–col.

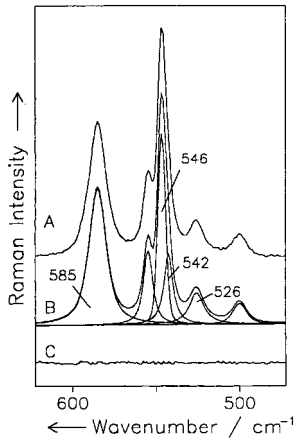

Figure 9. Analysis of the band pattern in the $\nu(Mo(O_2)_2)$ region of the Raman spectrum of **4**. A: measurement; B: band fit with fitted components; C: difference between fit and measurement.

Normal-coordinate analyses: For a precise assignment of the two A′ and A″ $\nu(M(O_2)_2)$ modes, simplified normal-coordinate analyses were carried out for the central molecular fragment $[MoO(O_2)_2LL']$ of the two structurally characterized compounds **4** and $[MoO(O_2)_2(hmpa)(OH_2)]$ (**9**) [17]. The ligands $OPtBu_3$, hmpa, and $OCMe_2$ were considered as point masses separated into the oxygen atom plus the remaining molecular fragment located at the phosphorus or carbon atom, respectively. The point mass of the water molecule is located at the oxygen atom. In a further simplification, only stretching coordinates are used, as shown in Figure 10. The coordinates s_1, s_2, and s_3 in an $Mo(O_2)$ triangle include bending character.

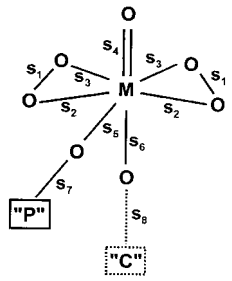

Figure 10. Internal coordinates of the central molecular fragment with L and L′ as point masses.

0947-6539/99/0511-3244 $ 17.50+.50/0 *Chem. Eur. J.* **1999**, *5*, No. 11

In the calculated force field optimized to the experimental vibrational data (Table 3) the coordinates s_1-s_3 and their interactions have similar values for both compounds. The force constant of the molybdenum–oxo bond s_4 (7.605 and 7.425 mdyn Å^{-1} for **4** and **9**, respectively) indicates a bond order between 2 and 3.[21] Due to the strong interaction between the two $Mo(O_2)$ triangles, small changes in the coordinates lead to large differences in the potential energy distribution (PED). Table 4 shows the PEDs for the calculated force fields listed in Table 3. The assignments of the (O–P), (Mo=O), and (O–O) stretching modes are confirmed by the percentage contributions of the internal coordinates to the respective vibrational motion. In the $\nu(M(O_2)_2)$ region the two polarized signals at about 550 and 585 cm^{-1} could be assigned to A′ $\nu_s(M(O_2)_2)$ and A′ $\nu_{as}(M(O_2)_2)$, respectively. The two A″ modes were found to be at approximately 540 cm^{-1} [$\nu_{as}(M(O_2)_2)$] and 520 cm^{-1} [$\nu_s(M(O_2)_2)$].

Table 3. Selected internal coordinates and force field of **9** and **4** (with HMPA, OH_2, $OPtBu_3$, and $OCMe_2$ as point masses).

Internal coordinates	Force constant type	Force constant[a] **9**	**4**
s_1	O–O stretch	3.356	3.362
s_2	M–O stretch	2.840	2.744
s_3	M–O stretch	2.649	2.761
s_4	M=O stretch	7.605	7.425
s_5	M–O_L stretch	2.341	2.375
s_6	M–$O_{L'}$ stretch	1.139	1.149
s_7	O_L–P_L stretch	6.937	6.536
s_8	$O_{L'}$–$C_{L'}$ stretch	-	11.758
interaction in the same [$M(O_2)$] triangle			
s_1s_2	O–O stretch/M–O stretch	−0.091	−0.090
s_1s_3	O–O stretch/M–O stretch	−0.103	−0.070
s_2s_3	M–O stretch/M–O stretch	−0.080	−0.089
interaction between both [$M(O_2)$] triangles			
s_1s_1'	O–O stretch/O–O stretch	−0.045	−0.030
s_2s_2'	M–O stretch/M–O stretch	0.652	0.518
s_3s_3'	M–O stretch/M–O stretch	0.153	0.159
s_2s_3'	M–O stretch/M–O stretch	0.239	0.242
interaction between the [$MO(O_2)_2$] unit and L or L′			
s_4s_6	M=O stretch/M–L′ stretch	0.063	0.054
s_2s_5	M–O stretch/M–L stretch	0.050	0.051
s_3s_5	M–O stretch/M–L stretch	0.050	0.050

[a] Values for stretches and their interactions are in mdyn Å^{-1}.

Table 4. Potential energy distribution (PED) for the stretching modes of the molecular fragment [$MoO(O_2)_2LL'$].

	Mode	Observed [cm^{-1}]	PED [%] s_1	s_2	s_3	s_4	s_5	s_6	s_7	s_8
		[$MoO(O_2)_2$(hmpa)(OH_2)] (**9**)								
A′	ν(O–P)	1121					15		85	
A′	ν(Mo=O)	972				99				
A′	ν(O–O)	876	85	8	6	1				
A″	ν(O–O)	865	89	6	5					
A′	$\nu_{as}(Mo(O_2)_2)$	586	1	49	49		1			
A′	$\nu_s(Mo(O_2)_2)$	552	16	33	48		2			
A″	$\nu_{as}(Mo(O_2)_2)$	534		56	44					
A″	$\nu_s(Mo(O_2)_2)$	519	4	52	44					
A′	ν(Mo–L′)	353					3	95	1	
A′	ν(Mo–L)	324			1		9	79	11	
		[$MoO(O_2)_2$($OPtBu_3$)($OCMe_2$)] (**4**)								
A′	ν(O–C)	1700						1		99
A′	ν(O–P)	1087					16		84	
A′	ν(Mo=O)	961				98				
A′	ν(O–O)	878	86	6	7	1				
A″	ν(O–O)	867	88	6	6					
A′	$\nu_{as}(Mo(O_2)_2)$	585	1	27	70		2			
A′	$\nu_s(Mo(O_2)_2)$	546	16	61	22		1			
A″	$\nu_{as}(Mo(O_2)_2)$	542		40	60					
A″	$\nu_s(Mo(O_2)_2)$	525	5	62	33					
A′	ν(Mo–L′)	333			1		29	64	6	
A′	ν(Mo–L)	323			1		53	40	6	

Raman spectra: Characteristic Raman bands of [$MoO(O_2)_2$-LL′] are listed in Table 3. The different donor ligands L affect the values of the A′ modes ν(O–O) and $\nu(M(O_2)_2)$ insignificantly. Characteristic changes are observed for the ν(Mo=O) mode, due to the donor ability of the ligand L′ *trans* to the oxo function. The donors L′ *trans* to the [Mo=O] function have an influence by reducing the molybdenum–oxygen bond order.[22] The highest wavenumbers for ν(Mo=O), indicating a higher Lewis acidity at the metal center, are found for the complexes with water or acetone molecules occupying the *trans* position. X-ray analyses of these complexes show a weak coordination between L′ and the metal center. The *cis* donor ligand L has a less significant effect on the Mo–O bond order of the oxo ligand. For [$MoO(O_2)_2L_2$] compounds the shift in the ν(Mo=O) mode could be used as a measure for the donor ability of L, which is demonstrated for compounds with L = $OPnOct_3$, $OPnDodec_3$, hmpa, and ON–col. According to the shift in the ν(Mo=O) mode the phosphane oxide ligands form weaker coordinative bonds to the metal center than hmpa and collidine *N*-oxide (Table 5).

Coordinatively saturated complexes have been considered; Raman spectra of unsaturated complex fragments will now be discussed, in order to elucidate their molecular structure.

Table 5. Band position [cm^{-1}] and assignments of the characteristic stretching vibrations of the $MoO(O_2)_2$ unit in complexes of type [$MoO(O_2)_2LL'$] and [$MoO(O_2)_2L_2$].

Assignments	[$MoO(O_2)_2LL'$] L = / L′ =	$OPMe_3$ / OH_2	$OPtBu_3$ / $OCMe_2$	HMPA / OH_2	[$MoO(O_2)_2L_2$] L =	$OPnOct_3$	$OPnDodec_3$	HMPA	ON–Col
A′ ν(Mo=O)		968 s	961 s	972 s		957 s	954 s	949 s	935 s
A′ ν(O–O)		875 s	878 s	876 s		877 s	877 m	876 m	880 m
A′ $\nu_{as}(Mo(O_2)_2)$		593 m	585 m	586 m		579 sh	582 w	582 m	585 sh
A′ $\nu_s(Mo(O_2)_2)$		546 s	546 s	552 s		536 s	539 m	539 s	540 m

Figure 11 shows Raman spectra in the $\nu(M(O_2)_2)$ region of the saturated complexes [$MoO(O_2)_2$(hmpa)(OH_2)], [$MoO(O_2)_2$-$(hmpa)_2$], and the coordinatively unsaturated complex [$MoO(O_2)_2$(hmpa)]. The band pattern in this region is characteristic for both types of complexes. The Raman spectra of [$MoO(O_2)_2LL'$] are dominated by the two A′ $\nu(M(O_2)_2)$ modes, in contrast to the spectra of comparable "[$MoO(O_2)_2L$]" complexes, which show at least three signals of equal intensity. Raman data of further compounds are listed in Table 6.

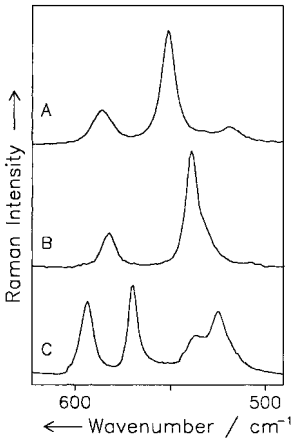

Figure 11. Raman spectra in the $\nu(Mo(O_2)_2)$ region of various bis(peroxo) complexes with hmpa as ligand.[1, 17] A: $[MoO(O_2)_2(hmpa)(OH_2)]$; B: $[MoO(O_2)_2(hmpa)_2]$; C: "$[MoO(O_2)_2(hmpa)]$".

Table 6. Band position [cm^{-1}] and assignments of the characteristic stretching vibrations of the $[MoO(O_2)_2]$ unit in the unsaturated complexes.

$[MoO(O_2)_2L]$ L = Assignments	HMPA	OP*t*Bu$_3$	OP*n*Oct$_3$	OP*n*Dodec$_3$	ON*n*Oct$_3$
ν(Mo=O)	973 s	970 s	974 s	977 s	972 s
ν(O–O)	878 s	883 s	882 s	885 s	873 s
$\nu(Mo(O_2)_2)$	594 m	586 m	592 m	594 m	589 m
	570 m	561 m	559 s	571 m	565 m
	538 sh			542 m	
	525 m	524 m	528 m	533 m	

Scheme 4 shows possible molecular structures, for which we expect characteristic changes in the vibrational spectra. Structure **I**, like $[MoO(O_2)_2LL']$, possesses C_s symmetry,

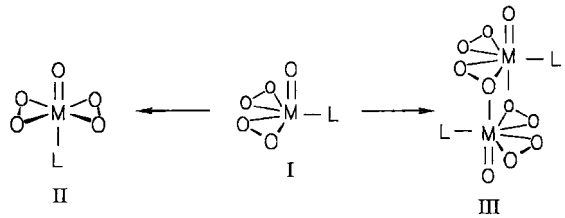

Scheme 4. Possible structures for which changes in the vibrational spectra are expected.

which should result in a similar Raman spectrum. For complex **II** we expect a simplification of the spectra due to the local D_{2h} symmetry of the $Mo(O_2)_2$ unit with a center of symmetry. A further possible way to stabilize the unsaturated species is by dimerization of two fragments forming a dinuclear complex **III** (Scheme 4). A bridging η^2:η^1 coordination of a peroxo unit was found previously in anionic compounds such as $[HO\{VO(O_2)_2\}_2]^{3-}$ or $[PO_4\{WO(O_2)_2\}_4]^{3-}$.[25, 26] The existence of structure **III** could explain the changes in the Raman spectra. The bonding situation of the two different peroxo ligands results in signals for the terminal and bridging units. For the bridging η^2-peroxo ligand the ν(O–O) mode should shift to higher wavenumbers, because the bonding of one oxygen atom to a second metal center leads to a further decrease in the electron density in the antisymmetric molecular orbital (LUMO) of the peroxo ligand. Nevertheless, the Raman spectra show no significant splitting in this region. All compounds possess a broad ν(O–O) band at higher wavenumbers than the analogous saturated complexes. The position of the ν(Mo=O) mode at around 975 cm^{-1} (Table 6) indicates a weak coordination of the bridging η^2-peroxo ligand *trans* to the oxo ligand. Precise assignment of the different $\nu(Mo(O_2))$ modes between 500 and 600 cm^{-1} is not yet possible. However, due to the complicated band structure in this region, a monomeric species of higher symmetry can be excluded.

DF calculations: To support our Raman spectroscopic results as well as the cryoscopic molecular weight determination for **2** we investigated the dimerization of peroxo complexes by computational methods. Firstly the suitability of DF methods describing the structurally defined model complex **4** was confirmed. Indeed, both the matchplots in Figure 12 and

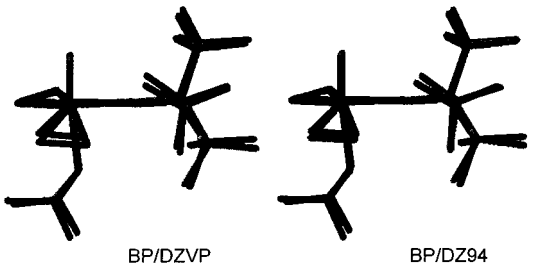

Figure 12. Matchplots of DF-calculated and X-ray-analyzed model complex **4**.

Table 7 show good agreement (RMS values: 0.227, 0.221) of the calculated (DZVP and DZ94) structure and the authentic peroxo complex characterized by X-ray analysis. Furthermore we focused on the complex fragment $[MoO(O_2)_2(OPtBu_3)]$ that is formed upon dissociation of the weakly bonded acetone ligand, which can be removed at 25 °C/10^{-2} mbar. Calculations based on DF methods (BLYP/DZVP) clearly favor the dimeric species **A2**: its energy minimum is 66 kJ mol^{-1} lower than that of the monomer **A1** (Figure 13). In this optimization *tert*-butyl groups in the model complex $[MoO(O_2)_2(OPtBu_3)]$ were replaced by methyl substituents.

These results clearly support indications in the Raman spectra of dimers of $[MoO(O_2)_2(OPtBu_3)]$ with lower symmetry and bridging peroxo groups. Although the μ^2,η^1:η^2-O_2

Table 7. Comparison of selected bond lengths [Å] and angles [°] of calculated complexes $[MoO_5(OPMe_3)]$ B1 and its dimer B2 with data from an X-ray analysis of **4**.

	Mo–O1	Mo–O7	Mo–O2	Mo-O4	Mo–O6	P–O7	Mo-O7-P
BLYP/DZVP	1.73	2.10	1.99	1.98	2.51	1.55	176.3
BLYP/DZ94	1.75	2.04	2.01	2.01	2.48	1.65	178.2
crystal structure **4**	1.67	2.03	1.94	1.92	2.45	1.51	175.7

0947-6539/99/0511-3246 $ 17.50+.50/0 *Chem. Eur. J.* **1999**, *5*, No. 11

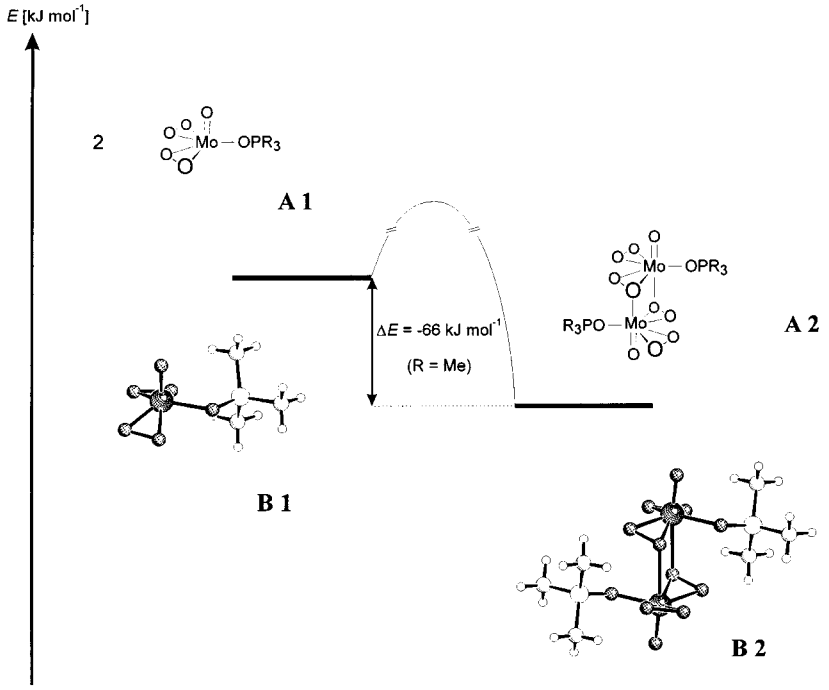

Figure 13. Structure and relative energy of calculated models **B1** and **B2** (R = Me) for complex fragment $[MoO_5(OPR_3)]$ **A1** and its dimer **A2** (R = *t*Bu) derived from **4**.

coordination mode is known for structurally well-defined anionic peroxometalates $[EO_4(WO_5)_4]^{n-}$ (E = P, S; $n = 2$, 3),[26, 27] there is no such structural example among neutral complexes of molybdenum and tungsten.

Why are dimers that should only exist in noncoordinating solvents such as chloroform better oxenoids than monomers with water or any other donor occupying the coordination site? One explanation may be that, in complexes with a $\mu^2,\eta^1{:}\eta^2$-peroxo ligand, one of the two peroxidic oxygen atoms is activated by two strong Lewis acidic centers of d^0 electronic configuration. We propose that this bonding situation makes the lower coordinate peroxidic oxygen atom a better oxenoid by increasing its electrophilicity and susceptibility to nucleophilic attack. Further theoretical and experimental studies will be focused on the polarization of the O–O bond of a peroxo ligand by additional protons, Lewis acid metal centers, silyl groups, and suchlike.

Could DF calculations possibly predict trends in the activity of the different ligands used in our experiments? A large set of physical properties of the ligands OER_3 was calculated by DF methods (PW91/TZVP) modeling the alkyl chains by methyl and ethyl groups. Surprisingly only one physical property, the proton affinity, was in good correlation with the observed catalytic activities (Table 8, Figure 14). Expecting that any correlation of a gas-phase property with the donor strength of the same base toward a Lewis acid in solution can only be a rough approximation, we were surprised that the proton affinity of the ligand matched perfectly with the catalyst activity under protic biphasic conditions.

Conclusions

The catalysts **1–3** show the highest activity in hydrogen peroxide activation reported so far for mononuclear molybdenum peroxides. The key to success is a combination of three processes in a biphasic epoxidation catalysis: the perhydrolysis of metal oxo functions; a phase-transfer step of neutral, not anionic, peroxo species; and the oxygen-transfer step. The catalytic activity of the oxidant system $[MoO(O_2)_2(OER_3)(H_2O)]$ (R = long-chain *n*-alkyl such as *n*-dodecyl; E = N, P, As) can be

Table 8. Proton affinities of ligands OER_3 (E = N, P, As; R = Me, Et) calculated by DF methods (PW91/TZVP).

Entry	L	Proton affinity (10^{-1} Hartree)
1	$ONMe_3$	3.5583
2	$OPMe_3$	3.5090
3	$OAsMe_3$	3.7230
4	$ONEt_3$	3.8060
5	$OPEt_3$	3.6209
6	$OAsEt_3$	3.8494

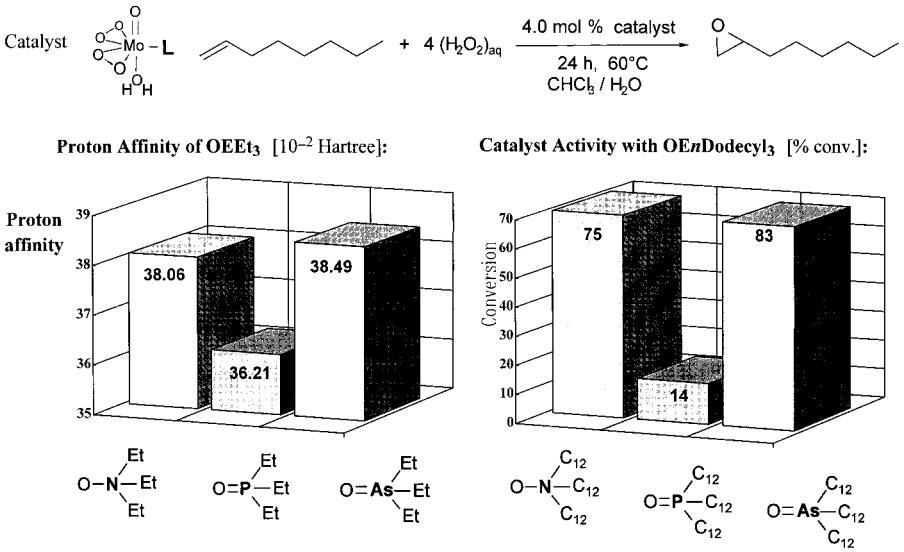

Figure 14. Correlation of the proton affinity of the ligands OER_3 (E = N, P, As) with the catalyst activity; comparison of data from Tables 1 and 8.

compared with other oxidant systems such as the homogeneous MTO/H_2O_2/*tert*-butyl alcohol system (Herrmann) or the biphasic systems with quarternary ammonium or pyridinium salts of heteropolyoxometalates of molybdenum and tungsten (Venturello, Ishii). Cryoscopy supported by Raman spectroscopic studies and DF calculations reveal good evidence that, promoted by the highly hydrophobic ligand regime, the catalytically active species $[MoO(O_2)_2(OER_3)]$ show a tendency in noncoordinating solvents to dimerize through bridging peroxo groups. In stoichiometric oxidations these dimers are active oxenoids toward olefins. The O transfer from an $[M(\eta^2\text{-}O_2)]$ functionality is slowed down or even inhibited in the presence of a second coordinating OER_3 or water ligand. Model reactions with complexes containing two amine oxide ligands or weakly coordinating hemilabile ether–arsane oxide and ether–phosphane oxide ligands reveal that much more active oxenoids are generated upon reaction of these peroxo species with either bis(trimethylsilyl) peroxide or H_2O_2. A free coordination site at a peroxo complex in combination with a highly hydrophobic ligand environment opens up mechanistic pathways involving peroxide—not olefin—activation, thus enabling a direct nucleophilic attack of the olefin HOMO at the lower coordinate oxygen atom of the oxenoid $[M(\eta^2\text{-}OOX)]$ (electrophile X = H^+, R^+, $SiMe_3^+$, d^0-metal Lewis acid). Our current investigations are aimed at mechanistic aspects of the O-transfer step and at broader applications of this biphasic oxidation system.

Experimental Section

General: The NMR spectra were recorded on a Bruker AC 200 (^{1}H at 200.1 MHz, ^{31}P at 81.0 MHz, ^{13}C at 50.3 MHz) at room temperature (25 °C), if not indicated otherwise. All ^{31}P and ^{13}C NMR spectra are proton broadband decoupled and the carbon multiplicities are not given. The methylene resonances in the ^{13}C NMR spectra were confirmed by DEPT measurements. The standards were CD_2Cl_2 (δ 5.32) and $CDCl_3$ (δ 7.24) for the ^{1}H NMR spectra, and CD_2Cl_2 (δ 54.20) and $CDCl_3$ (δ 77.00) for the ^{13}C NMR spectra. For the ^{31}P NMR spectra, 85 % H_3PO_4 served as external standard. Elemental analyses were performed in the microanalytical laboratories of Würzburg and Marburg Universities. The IR spectra were recorded on a Bruker IFS 25 with the software package Spektrafile IR Plus (Heyden & Son GmbH) and on a Perkin-Elmer 283 or 1420. The solids were recorded as Nujol mulls between KBr plates. Raman spectra were excited with the 647.1 nm line of a krypton ion laser (Spectra Physics model 2025). The scattered light was dispersed by means of a SPEX model 1404 double monochromator and detected with a charge coupled device (CCD) camera system (Photometrics, model RDS 2000) employing the scanning multichannel technique.[28] Raman spectra of the peroxo complexes were measured with a microscope setup and sample materials were handled under an argon atmosphere. Assignments are given for some valence (ν), deformation (δ), and twist (τ) vibrations, with the subscripts "s" for symmetric, "as" for antisymmetric, "ip" for in-plane, and "oop" for out-of-plane. All band positions are given in cm^{-1}. The samples from the catalytic epoxidations of 1-octene were analyzed by GC on a Carlo Erba HRGC 5300 instrument, equipped with a fused-silica column (5 m × 0.53 mm i.d.), DB-5 (25 m × 0.32 mm × 0.52 μm; J & W Scientific), and FI detector, with di(*n*-butyl) ether as internal standard.

Computations: DF methods were used, because of their moderate demand on CPU time (scaling factor $N^{2.2-3}$ with N basis functions) and because of their ability to describe transition metal complexes in good agreement with experimental data.[29] DF calculations were performed on CRAY T90 and SGI R4400 computers by means of DGAUSS 3.0[30, 31] and DEMON 1.03 software.[32] The DF is based on Hohenberg and Kohn's theorem[33] that the ground-state energy $E[\rho]$ of a system is an exact functional of the electron density ρ: $E[\rho] = T[\rho] + U[\rho] + E_{xc}[\rho]$, where T is the kinetic energy of noninteracting electrons, U the Coulomb potential, and E_{xc} the exchange correlation energy. For the geometry optimization of the metal complexes **4, B1**, and **B2** the exchange correlation energy functional BLYP (DGAUSS program) was used. All optimizations of the transition metals were performed using the DZVP[34, 35] basis set. The electronic density and the exchange correlation potential were fitted by a triple-zeta A1 set. The ground-state structures were determined by the standard optimization technique,[36] as implemented in DGAUSS.

Proton affinities were calculated as energy differences of the protonated and neutral ligands. Energies were obtained by optimization of the corresponding ligands with the PW91/TZVP functional basis set combination within the DEMON program. RMS values were determined by the fit atom algorithm of the SYBYL[37] program package.

Normal-coordinate analyses (NCAs) have been performed for the central molecular fragment of two complexes to confirm our assignments in the metal–oxygen stretching region of the vibrational spectra. Force field calculations were carried out on a personal computer with a modified version of the program package QCMP-067[38] and VIA,[39] working on the basis of Wilson's GF-matrix method.[40] The structural parameters have been taken from X-ray analyses with averaged bond lengths and angles, due to the C_s symmetric structure of the complexes.

Materials: The following compounds were commercially available or prepared as described in the literature: N*n*Dodec$_3$ (Merck), OP*n*Oct$_3$ (Fluka), OP*n*Dodec$_3$,[41] OP*t*Bu$_3$,[42] As*n*Dodec$_3$,[43] *i*Pr$_2$PCH$_2$CH$_2$OMe,[44] *i*Pr$_2$AsCH$_2$CH$_2$OMe,[45] [MoO$_5$(OP*t*Bu$_3$)],[15] [MoO$_5$(hmpa)(H$_2$O)],[1] [MoO$_5$(hmpa)$_2$],[1] [MoO$_5$(hmpa)],[1] [MoO$_5$(OPMe$_3$)(H$_2$O)],[2] and the stock solution of $[MoO_5(H_2O)_2]_{aq}$.[1]

Ligands OE*n*Dodec$_3$ (E = N, As): To amine or arsane E*n*Dodec$_3$ (1 equiv) dissolved in diethyl ether, aqueous hydrogen peroxide (30 %; 5 equiv) was added dropwise. The mixture was stirred for three days at 30 °C (amine)/3 h at 25 °C (arsane). Excess hydrogen peroxide was decomposed by adding traces of MnO_2, the organic phase was separated and the solvent was evaporated. The white products were spectroscopically pure (^{13}C NMR) but were crystallized from acetonitrile for the elemental analyses.

ONndodec$_3$: White solid; yield: 94 %; DTA: 60 °C (endothermic), 78 °C (exothermic); $C_{36}H_{75}NO$ (538.0): calcd C 80.37, H 14.06, N 2.60; found C 80.00, H 13.90, N 2.61.

OAsndodec$_3$: White solid; yield: 89 %; DTA: 71 °C (endothermic); $C_{36}H_{75}AsO$ (598.9): calcd C 72.18, H 12.62; found C 72.38, H 12.33.

Ligands *i*Pr$_2$E(O)CH$_2$CH$_2$OMe (E = P, As): To 1.0 equiv phosphane or arsane dissolved in diethyl ether was added dropwise 1.2 equiv aqueous hydrogen peroxide (30 %). The mixture was stirred for 3 h at 0 °C. Excess hydrogen peroxide was decomposed by adding traces of MnO_2, the organic phase was separated, and the solvent was evaporated. Both ligands are colorless oils. They were spectroscopically pure (^{13}C NMR) and used without further purification. Yields: 85 % (phosphane oxide), 76 % (arsane oxide).

[MoO$_5$(ON*n*Dodec$_3$)] (1): MoO_3 (413 mg, 2.87 mmol) was suspended in H_2O_2 (30 %; 3.27 mL, 28.7 mmol) at 40 °C for 4 h. After a clear yellow solution had formed, N*n*Dodec$_3$ (570 mg, 1.61 mmol) dissolved in CH_2Cl_2 (5 mL) was added dropwise. After being stirred for 5 h at 25 °C the organic phase was separated and washed with water (3 × 5 mL). The CH_2Cl_2 solution was evaporated to dryness (25 °C/10^{-2} mbar). The residue was washed with water (2 × 2 mL) and dried for 6 h at 25 °C/5 × 10^{-5} mbar to yield a pale yellow solid. Yield: 2.81 g (95 %); differential thermal analysis (DTA): 75 °C (decomp); ^{1}H NMR (400.1 MHz, $CDCl_3$, 25 °C, TMS): δ = 0.86 (t, 9H, CH_3, ^2J(H, H) = 7.2 Hz), 1.18–1.43 (m, 54H, CH_2 (3–11)), 1.68–1.87 (m, 6H, CH_2 (2)), 3.40–3.67 (m, 6H, CH$_2$ (1)); ^{13}C NMR (100.6 MHz, $CDCl_3$, 25 °C, TMS): δ = 14.0 (*C*H$_3$), 22.7, 26.2, 29.0, 29.2, 29.3, 29.4, 29.4, 29.5, 29.6 (*C*H$_2$ (3–11)), 31.9 (*C*H$_2$ (2)), 64.2 (*C*H$_2$ (1)); IR (Nujol): $\tilde{\nu}$ = 1639 (w), 1521 (m), 1320 (w), 977 (vs) [ν(Mo–O)], 858 (vs) [ν(O–O)], 800 (w), 718 (m), 643 (s), 592 (s) [ν(Mo(O$_2$)$_2$)], 542 (m) [ν(Mo(O$_2$)$_2$)], 538 (m) [ν(Mo(O$_2$)$_2$)], 509 (w); $C_{36}H_{75}MoNO_6$ (713.9): calcd C 60.57, H 10.59, N 1.96; found C 60.62, H 10.72, N 1.95.

[MoO$_5$(OP*n*Dodec$_3$)] (2): Prepared analogously to **1**: Raman (wax): $\tilde{\nu}$ = 1441 (s) [δ(CH)], 1299 (s) [τ(CH$_2$)], 1129 (w) [ν(C–C)], 1084 (m) [ν(O–P)], 1065 (m) [ν(C–C)], 954 (m) [ν(Mo–O)], 885 m [ν(O–O)], 594 (w) [ν(Mo(O$_2$)$_2$)], 571 (w) [ν(Mo(O$_2$)$_2$)], 533 (m) [ν(Mo(O$_2$)$_2$)], 353 (m), 328

0947-6539/99/0511-3248 $ 17.50+.50/0 *Chem. Eur. J.* **1999**, *5*, No. 11

(w); cryoscopic molecular weight determination (cyclohexane): 1397; calcd for dimer $[C_{36}H_{75}MoO_6P]_2$: 1461.8.

[MoO_5(OAs*n*Dodec$_3$)] (3): MoO_3 (263 mg, 1.83 mmol) was suspended in H_2O_2 (30%; 1004 mL, 28.7 mmol) at 40°C for 4 h. After a clear yellow solution had formed, OAs*n*Dodec$_3$ (1.08 g, 1.80 mmol) dissolved in $CHCl_3$ (4 mL) was added dropwise. After being stirred for 16 h at 25°C the organic phase was separated and washed with water (3×5 mL). The $CHCl_3$ solution was evaporated to dryness (25°C/10^{-2} mbar). The yellow residue was dried for 10 h at 25°C/5×10^{-5} mbar to give a pale yellow wax. Yield: 1.35 g (97%); DTA: 112°C (decomp); ^{1}H NMR (200.1 MHz, $CDCl_3$, 25°C, TMS): $\delta=0.84$ (t, 9H, (CH_3), ^3J(H, H) = 6.7 Hz), 1.10–1.45 (br, 54H, CH_2 (3–11)), 1.60–1.85 (br, 6H, CH_2 (2)), 2.60–2.83 (br, 6H, CH_2 (1)); ^{13}C NMR (50.3 MHz, $CDCl_3$, 25°C, TMS): $\delta=14.6$ (CH_3), 22.9, 23.2, 28.1, 29.0, 29.6, 29.7, 29.9, 30.2, 31.4 (CH_2 (3–11)), 30.9 (CH_2 (2)), 32.4 (CH_2 (1)); IR (Nujol): $\tilde{\nu}=1258$ (w), 1077 (br), 954 (w) [ν(Mo–O)], 908 (br) [ν(As–O)], 835 (w) [ν(O–O)], 797 (br), 713 (w), 580 (w) [ν(Mo(O_2)$_2$)]; $C_{36}H_{75}AsMoO_6$ (774.8): calcd C 55.81, H 9.76; found C 55.62 H 9.79.

[MoO_5(OP*t*Bu$_3$)(OCMe$_2$)] (4): [MoO_5(OP*t*Bu$_3$)][15] (665 mg, 1.69 mmol) was dissolved in $CHCl_3$/acetone (2 mL, 2:1). The yellow solution was cooled to −60°C and maintained at this temperature for five days. Yellow crystals were obtained. Yield: 52% (400 mg); DTA: 59°C (m.p.), 140°C (decomp); ^{1}H NMR (200.1 MHz, CD_2Cl_2, 25°C, TMS): $\delta=1.56$ (d, 27H, C(CH_3)$_3$, ^3J(P, H) = 13.9 Hz), 2.09 (s, 6H, OC(CH_3)$_2$); ^{13}C NMR (50.3 MHz, CD_2Cl_2, 25°C, TMS): $\delta=29.4$ (s, C(CH_3)$_3$), 31.3 (OC(CH_3)$_2$), 41.5 (d, $C(CH_3)_3$, ^1J(C, P) = 45.0 Hz), 207.3 (OC(CH$_3$)$_2$); ^{31}P NMR (81.0 MHz, CD_2Cl_2, 25°C, H_3PO_4): $\delta=95.7$ (s); IR (Nujol): $\tilde{\nu}=1620$ (m) [ν(C–O)], 1195 (s), 1075 (vs) [ν(P–O)], 1020 (m), 960 (vs) [ν(Mo–O)], 941 (m), 930 (m), 879 (vs) [ν(O–O)], 712 (m), 655 (s), 636 (vs), 590 (s) [A′ ν_{as}(Mo(η^2-O_2)$_2$)], 552 (m) [A′ ν_s(Mo(η^2-O_2)$_2$)], 519 (s) [A″ ν_s(Mo(η^2-O_2)$_2$)], 496 (s), 423 (m); Raman (polycrystalline): $\tilde{\nu}=1087$ (m) [ν(O–P)], 961 (vs) [ν(Mo–O)], 878 (vs) [A′ ν(O–O)], 811 (m) [ν(C–C)], 585 (m) [A′ ν_{as}(Mo(η^2-O_2)$_2$)], 555 (m) [ν_s(PC_3)], 546 (s) [A′ ν_s(Mo(η^2-O_2)$_2$)], 542 (w) [A″ ν_{as}(Mo(η^2-O_2)$_2$)], 525 (w) [A″ ν_s(Mo(η^2-O_2)$_2$)], 323 (m), 316 (m); $C_{15}H_{33}MoO_7P$ (452.3): calcd C 39.83, H 7.35; found C 39.70, H 7.34.

[MoO_5{*i*Pr$_2$P(O)CH$_2$CH$_2$OCH$_3$}] (5): MoO_3 (634 mg, 1.50 mmol) was suspended in H_2O_2 (30%; 0.84 mL, 7.50 mmol) at 40°C for 4 h. After a clear, yellow solution had formed, *i*Pr$_2$P(O)CH$_2$CH$_2$OCH$_3$ (269 mg, 1.40 mmol) was added. The reaction mixture was stirred for 3 h and extracted with CH_2Cl_2 (3×5 mL) and the combined extracts were evaporated to dryness (25°C/10^{-2} mbar). The pale yellow residue was washed with pentane (2×3 mL) and dried for 3 h at 25°C/5×10^{-5} mbar to give a yellow solid. Yield: 316 mg (61%); DTA: 123°C (decomp); ^{1}H NMR (200.1 MHz, CD_2Cl_2, 25°C, TMS): $\delta=1.35$ (dd, 6H, P–CH(CH_3)$_A$, ^3J(H, H) = 7.31 Hz, ^3J(P, H) = 2.56 Hz), 1.44 (dd, 6H, P–CH(CH_3)$_B$, ^3J(H, H) = 7.31 Hz, ^3J(P, H) = 1.83 Hz), 2.25 (dt, 2H, P–CH_2CH$_2$OCH$_3$, ^2J(P, H) = 8.40 Hz, ^3J(H,H) = 6.21 Hz), 2.39–2.59 (m, 2H, P–CH(CH$_3$)$_2$), 3.09 (s, 3H, P–CH$_2$CH$_2$OCH_3), 3.68 (dt, 2H, P–CH$_2$$CH_2OCH_3$, ^3J(P, H) = 17.9 Hz, ^3J(H,H) = 6.21 Hz); ^{13}C NMR (50.1 MHz, CD_2Cl_2, 25°C, TMS): $\delta=15.4$ (P–CH(CH_3)$_A$), 15.5 (P–CH(CH_3)$_B$), 20.6 (d, P–CH_2CH$_2$OCH$_3$, ^1J(P, C) = 56.8 Hz), 26.0 (d, P–CH(CH$_3$)$_2$, ^1J(P, C) = 63.0 Hz), 59.9 (P–CH$_2$$CH_2OCH_3$), 66.4 (P–$CH_2CH_2OCH_3$, ^2J(P, C) = 63.0 Hz); ^{31}P NMR (81.0 MHz, $CDCl_3$, 25°C): $\delta=$ 86.1 (s); IR (Nujol): $\tilde{\nu}=1190$ (m), 1097 (vs) [ν(P–O)], 940 (s) [ν(Mo–O)], 799 (s), 875 (m) [ν(O–O)], 702 (m), 660 (m), 629 (m), 585 (s) [A′ ν_{as}(Mo(η^2-O_2)$_2$)], 548 (m) [A′ ν_s(Mo(η^2-O_2)$_2$)], 494 (m), 440 (m), 419 (m); $C_9H_{21}MoO_7P$ (368.2): calcd C 29.19, H 5.72; found C 29.48, H 5.58.

[MoO_5{*i*Pr$_2$As(O)CH$_2$CH$_2$OCH$_3$}] (6): MoO_3 (845 mg, 2.00 mmol) was suspended in 30% H_2O_2 (1.12 mL, 10.0 mmol) at 40°C for 4 h. After a clear, yellow solution had formed, *i*Pr$_2$As(O)CH$_2$CH$_2$OCH$_3$ (425 mg, 1.80 mmol) was added. The reaction mixture was stirred for 3 h at 10°C. After extraction with CH_2Cl_2 (6×20 mL) the combined extracts were evaporated to dryness (25°C/10^{-2} mbar). The pale yellow residue was washed with pentane (2×3 mL) and dried for 3 h at 25°C/5×10^{-5} mbar to give a yellow solid. Yield: 395 mg (53%); DTA: 102°C (decomp); ^{1}H NMR (200.1 MHz, $CDCl_3$, 25°C, TMS): $\delta=1.47$ (d, 6H, As–CH(CH_3)$_A$, ^3J(H, H) = 7.31 Hz), 1.48 (d, 6H, As–CH(CH_3)$_B$, ^3J(H, H) = 6.94 Hz), 2.75 (t, 2H, As–CH_2CH$_2$OCH$_3$, ^3J(H, H) = 6.21 Hz), 2.97 (sept, 2H, As–CH(CH$_3$)$_2$, ^3J(H, H) = 7.31 Hz), 3.37 (s, 3H, As–CH$_2$CH$_2$OCH_3), 3.70 (t, 2H, As–CH$_2$$CH_2OCH_3$, ^3J(H, H) = 6.21 Hz); ^{13}C NMR (50.1 MHz, $CDCl_3$, 25°C, TMS): $\delta=16.5$ (As–CH(CH_3)$_A$), 16.6 (As–CH(CH_3)$_B$), 24.8 (As–CH_2CH$_2$OCH$_3$), 33.6 (As–CH(CH$_3$)$_2$), 59.3 (As–CH$_2$CH$_2$OCH_3), 66.0 (As–CH$_2$$CH_2OCH_3$); IR (Nujol): $\tilde{\nu}=1297$ (m), 1244 (m), 1184 (w), 1166 (m), 1056 (m), 960 (s) [ν(MoO)], 902 (m), 881 (s) [ν(As–O)], 840 (s) and 831 [ν(O–O)], 766 (m), 719 (s), 637 (m), 578 (m) [A′ ν_{as}(Mo(η^2-O_2)$_2$)], 538 (m) [A′ ν_s(Mo(η^2-O_2)$_2$)]; $C_9H_{21}AsMoO_7$ (412.1): calcd C 25.99, H 5.10, As 18.10; found C 26.09, H 5.11, As 17.80.

[MoO_5(OP*n*Dodec$_3$)$_2$] (7): MoO_3 (371 mg, 2.58 mmol) was suspended in H_2O_2 (30%; 3.00 mL, 27.6 mmol) at 40°C for 4 h. After a clear, yellow solution had formed, THF (4.0 mL) and OP*n*Dodec$_3$ (2.86 g, 5.16 mmol) was added. After 2 h the mixture was evaporated to a volume of 3 mL and extracted with CH_2Cl_2 (3×5 mL). The combined extracts were evaporated to dryness (25°C/10^{-2} mbar). The yellow waxy residue was washed with water (2×2 mL) and dried for 6 h at 25°C/5×10^{-5} mbar to give a yellow wax. Yield: 3.20 g (97%); DTA: 39°C (m.p.), 119°C (decomp); ^{1}H NMR (200.1 MHz, C_6D_6, 25°C, TMS): $\delta=0.92$ (t, 18H, CH_3, ^3J(H, H) = 6.2 Hz), 1.20–1.45 (br, 120H, CH_2–(2–11)), 1.40–2.05 (br, 12H, CH_2)(1)); ^{13}C NMR (50.3 MHz, C_6D_6, 25°C, TMS): $\delta=14.4$ (s, CH_3)), 22.0 (br, CH_2(2)), 26.3 (d, CH_2(1), ^1J(P, C) = 85.2 Hz), 23.1, 29.5, 29.6, 29.7, 30.1, 30.2, 30.2, 32.4 (all s, CH_2(4–11)), 31.5 (d, CH_2(3), ^3J(P, C) = 14.8 Hz); ^{31}P NMR (81.0 MHz, C_6D_6, 293 K, H_3PO_4): $\delta=77.4$ (OP_{eq}), 57.4 (OP_{ax}); ^{31}P NMR (81.0 MHz, C_6D_6, $T_C=363$ K, H_3PO_4): $\delta=66.5$ (coalescence OP_{eq}, OP_{ax}); IR (Nujol): $\tilde{\nu}=1295$ (m), 1259 (m), 1133 (m) and 1085 (s) [ν(P–O)], 952 (vs) [ν(Mo–O)], 872 (s) and 861 (vs) [ν(O–O)], 797 (s), 716 (m), 651 (m), 579 (s) [A′ ν_{as}(Mo(η^2-O_2)$_2$)], 555 (m) [A′ ν_s(Mo(η^2-O_2)$_2$)]; Raman (polycrystalline): $\tilde{\nu}=1440$ (m) [δ(CH)], 1298 (s) [τ(CH_2)], 1130 (w) [ν(C–C)], 1085 (w) [ν(O–P)], 1065 (m) [ν(C–C)], 954 (s) [ν(Mo–O)], 877 s [A′ ν(O–O)], 582 (w) [A′ ν_{as}(Mo(η^2-O_2)$_2$)], 539 (m) [A′ ν_s(Mo(η^2-O_2)$_2$)], 327 (m); $C_{72}H_{150}MoO_7P_2$ (1285.9): calcd C 67.25 H 11.76; found C 67.13 H 11.23.

[MoO_5(OP*n*Oct$_3$)$_2$]: Prepared analogously to **7**. Raman (oil): $\tilde{\nu}=1439$ (s) [δ(CH)], 1305 (m) [τ(CH_2)], 1119 (w) [ν(C–C)], 1081 (w) [ν(O–P)], 1065 (w) [ν(C–C)], 957 (s) [ν(Mo–O)], 877 s [A′ ν(O–O)], 579 (sh) [A′ ν_{as}(Mo(η^2-O_2)$_2$)], 536 (s) [A′ ν_s(Mo(η^2-O_2)$_2$)], 324 (m).

[MoO_5(OP*n*Oct$_3$)]:[15] Raman (oil): $\tilde{\nu}=1440$ (s) [δ(CH)], 1303 (s) [τ(CH_2)], 1121 (w) [ν(C–C)], 1081 (w) [ν(O–P)], 1066 (w) [ν(C–C)], 974 (s) [ν(Mo–O)], 882 (s) [A′ ν(O–O)], 592 (m) [ν(Mo(O_2)$_2$)], 559 (s) [ν(Mo(O_2)$_2$)], 528 (m) [ν(Mo(O_2))], 328 (m), 305 (m).

[MoO_5(ON*n*Oct$_3$)]:[15] Raman (oil): $\tilde{\nu}=1451$ (s,br) [δ(CH)], 1305 (m,br) [τ(CH_2)], 1128 (w) [ν(C–C)], 1082 (m), 1067 (m) [ν(C–C)], 972 (m, br) [ν(Mo–O)], 873 (m) [A′ ν(O–O)], 589 (m) [ν(Mo(O_2)$_2$)], 565 (m) [ν(Mo(O_2)$_2$)], 542 (m) [ν(Mo(O_2)$_2$)], 319 (m), 299 (m).

[MoO_5(ONcol)$_2$] (8): MoO_3 (660 mg, 4.59 mmol) was suspended in H_2O_2 (30%; 3.00 mL, 27.6 mmol) at 40°C for 4 h. After a clear, yellow solution had formed, collidine *N*-oxide (1.26 g, 9.19 mmol) was added. After 1 h of stirring at 25°C a yellow solid started to precipitate. The solution was filtered and the remaining yellow residue was washed with water ($2\times$ 1 mL) at 5°C, then CH_2Cl_2 (3×2 mL) at 0°C, and dried for 4 h at 25°C/ 5×10^{-5} mbar to give a yellow solid. Yield: 1.95 g (95%); DTA: 153°C (decomp); ^{1}H NMR (200.1 MHz, CD_2Cl_2, 25°C, TMS): $\delta=2.42$ (s, 12H, col–(CH_3)$_o$), 2.73 (s, 6H, col–(CH_3)$_p$), 7.19 (s, 4H, col–H); ^{13}C NMR (50.3 MHz, CD_2Cl_2, 25°C, TMS): $\delta=19.0$ (col–(CH_3)$_o$), 21.3 (col–(CH_3)$_p$), 126.8 (col–C(3,5)), 127.2 (col–C(4)), 152.3 (col–C(2,6)); IR (Nujol): $\tilde{\nu}=1631$ (s) and 1571 (s) [ν(C=C)], 1259 (w), 1195 (vs) [ν(N–O)], 1156 (s), 1029 (m), 1012 (m), 924 (vs) [ν(Mo–O)], 873 (s) and 861 (vs) [ν(O–O)], 780 (vs) [$\nu(CH_{ar})_{oop}$], 710 (m), 648 (s), 583 (vs) [A′ ν_{as}(Mo(η^2-O_2)$_2$)], 535 (w) [A′ ν_s(Mo(η^2-O_2)$_2$)], 517 (w), 499 (w), 454 (w); Raman (polycrystalline): $\tilde{\nu}=1636$ (m) [ν(C–C)], 1329 (m) [δ(CH_3)], 1329 (m) [δ_{ip}(CH)], 935 (s) [ν(Mo–O)], 880 (m) [A′ ν(O–O)], 868 (vw) [A″ ν(O–O)], 601 (s), 594 s, 585 (sh) [A′ ν_{as}(Mo(η^2-O_2)$_2$)], 567 (w), 540 (s) [A′ ν_s(Mo(η^2-O_2)$_2$)], 316 (m); $C_{16}H_{22}MoN_2O_7$ (450.3): calcd C 42.68 H 4.92 N 6.22; found C 41.62 H 4.97 N 5.91.

X-ray structure analysis of 4: $C_{15}H_{33}MoO_7P$, $M_r=452.32$, monoclinic, space group $P2_1/n$, $a=8.586(4)$, $b=14.707(3)$, $c=16.334(7)$ Å, $\beta=99.7°$, $V=2032.9(14)$ Å^3, $Z=4$, $\rho_{calcd}=1.478$ g cm^{-3}, $\lambda(Mo_{K\alpha})=0.70930$ Å, $\mu=0.754$ mm^{-1}, $T=223$ K. Data collection and reduction: A yellow crystal $0.50\times0.40\times0.20$ mm^{-3} was used to record 2865 intensities to $2\Theta_{max}=44.86°$ (Enraf–Nonius CAD4 diffractometer), of which 2654 were unique ($R_{int}=0.0011$). An absorption correction was applied on the basis of ψ scans, with the transmission minimum at 92.15%. Structure solution and refinement: The structure was solved by direct methods (SHELXS-86)[46] and subjected to full-matrix least-squares refinement on F^2 (SHELXL-

93),[47] All non-hydrogen atoms were refined anisotropically. The methyl C atoms of *tert*-butyl groups were disordered and refined isotropically without H atoms. All H atoms in the acetone ligand were refined isotropically using the difference Fourier technique. Refinement proceeded to $R_w(F^2) = 0.118$ for 2654 reflections, conventional $R(F) = 0.042$ and maximum $\Delta\rho = 0.62$ e Å^{-3}.

X-ray structure analysis of 5: $C_9H_{21}MoO_7P$, $M_r = 368.17$, monoclinic, space group $P2_1$, $a = 12.930(1)$, $b = 7.516(1)$, $c = 15.114(1)$ Å, $\beta = 99.8°$, $V = 1447.4(2)$ Å^3, $Z = 4$, $\rho_{calcd} = 1.690$ g cm^{-3}, $\lambda(Mo_{K\alpha}) = 0.71073$ Å, $\mu = 1.038$ mm^{-1}, $F(000) = 752$, $T = 223$ K. Data collection and reduction: A yellow crystal $0.40 \times 0.30 \times 0.30$ mm^{-3} was used to record 3376 intensities to $2\Theta_{max} = 50.08°$ (Enraf – Nonius CAD4 diffractometer), of which 2539 were unique ($R_{int} = 0.0285$). Non-absorption correction was used, with the minimum of transmission at 77.96%. Structure solution and refinement: The structure was solved by direct methods (SHELXS-96)[48] and subjected to full-matrix least-squares refinement on F^2 (SHELXL-96).[49] All non-hydrogen atoms were refined anisotropically. All H atoms were found and refined isotropically using the difference Fourier technique. Refinement proceeded to $R_w(F^2) = 0.0659$ for 2539 reflections, conventional $R(F) = 0.0230$ and maximum $\Delta\rho = 0.338$ e Å^{-3}.

X-ray structure analysis of 6: $C_9H_{21}AsMoO_7$, $M_r = 412.12$, monoclinic, space group $P2_1/c$, $a = 21.632(4)$, $b = 7.570(2)$, $c = 27.524(5)$ Å, $\beta = 103.172(12)°$, $V = 4388.(2)$ Å^3, $Z = 12$, $\rho_{calcd} = 1.871$ g cm^{-3}, $\lambda(Cu_{K\alpha}) = 1.54187$ Å, $\mu = 10.074$ mm^{-1}, $F(000) = 2472$, $T = 203$ K. Data collection and reduction: A yellow crystal $0.30 \times 0.25 \times 0.23$ mm^{-3} was used to record 5841 intensities to $2\Theta_{max} = 55.90°$, of which 5661 were unique ($R_{int} = 0.0474$). An absorption correction was applied empirically (SHELXA) with the minimum of transmission at 37.0%. Structure solution and refinement: The structure was solved and subjected to full-matrix least-squares refinement on F^2 (SHELXA). All non-hydrogen atoms were refined anisotropically, and H atoms were included using a riding model or rigid methyls. Refinement proceeded to $R_w(F^2) = 0.1267$ for 5841 reflections, conventional $R(F) = 0.0600$ and maximum $\Delta\rho = 0.451$ e Å^{-3}.

SCHAKAL-92[50] was used for presentation of the molecular structures.

Further details of the crystal structure investigations can be obtained from the Fachinformationszentrum Karlsruhe, D-76344 Eggenstein-Leopoldshafen (Germany) (fax: (+49) 7247-808-666; e-mail: crysdata@fiz.karlsruhe.de), on quoting the depository numbers CSD-408410, CSD-408411, and CSD-408412.

Stoichiometric oxidations of 1-octene with [MoO_5(ON*n*Dodec$_3$)] (1):

Run B: A stock solution of 1-octene (0.312 M in $CHCl_3$, 1.00 mL, 0.312 mmol) was added at 25 °C to [MoO_5(ON*n*Dodec$_3$)] (229 mg, 0.312 mmol) dissolved in $CHCl_3$ (3.0 mL). The mixture was heated to 60 °C and stirred for 16 h at this temperature. The sample was analyzed directly by GC without workup (internal standard di(*n*-butyl) ether).

Run A: The conversion was followed after addition of 4 equiv H_2O_2 (1.25 mmol, 142 mg of a 30% solution in water) to the run B mixture.

Run C: The conversion was followed after addition of 150 mg water to the mixture of run B.

Stoichiometric oxidations of 1-octene with [MoO_5(ON*n*Dodec$_3$)] (1) + ON*n*Dodec$_3$:

Run B: A stock solution of 1-octene (0.312 M in $CHCl_3$, 1.00 mL, 0.312 mmol) was added at 25 °C to [MoO_5(ON*n*Dodec$_3$)] (229 mg, 0.312 mmol) and ON*n*dodec$_3$ (168 mg, 0.312 mmol) dissolved in $CHCl_3$ (3.0 mL). The mixture was heated to 60 °C and stirred for 16 h at this temperature. The sample was analyzed directly by GC without workup (internal standard di(*n*-butyl) ether).

Run A: The conversion was followed after addition of 4 equiv H_2O_2 (1.25 mmol, 142 mg of a 30% solution in water) to the mixture of run B.

Run C: The conversion was followed after addition of 150 mg water to the mixture of run B.

Catalytic epoxidation of 1-octene: An aqueous stock solution of [$MoO(O_2)_2(H_2O)_2$] containing peroxomolybdic acid (1.39 mmol g^{-1}) was prepared.[1] Ligands were added from stock solutions in $CHCl_3$ (0.144 mmol mL^{-1}).

Experiments 1 – 3 (molar ratio 1-octene/H_2O_2/catalyst = 1:4:0.04): H_2O_2 (30% in H_2O; 4.08 g, 36.0 mmol) and OE*n*Dodec$_3$ (E = N, P, As; 0.36 mmol) dissolved in $CHCl_3$ (2.5 mL) were added to the freshly prepared stock solution of [$MoO(O_2)_2(H_2O)_2$] (259 mg, 0.36 mmol). The pH of the aqueous peroxomolybdic acid phase was 3.0. After the mixture had been stirred for 5 min at 60 °C, di(*n*-butyl) ether (250 mg, 1.92 mmol, internal standard) and 1-octene (1.01 g, 9.0 mmol) were added. The biphasic mixture was stirred magnetically with a Teflon-coated bar in a 15 mm glass tube while the temperature was maintained at 60 °C. The conversion was monitored by GC.

A similar procedure using the inverse molar ratios was applied for experiments 4 – 6 (1-octene/H_2O_2/catalyst = 4:1:0.01) and for experiments 7 – 9 (cyclooctene/H_2O_2/catalyst = 4:1:0.005).

Catalytic epoxidation of 1-octene with 4 mol% catalyst based on olefin: Molybdenum trioxide (Fluka, 260 mg, 1.80 mmol) was added to tris(dodecyl)amine (Merck, 930 mg, 1.80 mmol), hydrogen peroxide (30%, 25.2 g, 223 mmol), and chloroform (20 mL). Within 20 min of stirring at 25 °C the organic phase became yellow. 1-Octene (5.04 g, 45.0 mmol) was added to the biphasic catalyst system. After 24 h of stirring at 25 °C (73% conversion of olefin) a second portion of hydrogen peroxide (30%, 25.2 g, 223 mmol) was added and the mixture was stirred for another 24 h at 25 °C to achieve 98% conversion. The yellow organic layer was separated and washed with 3×15 mL water. Volatiles at 55 °C/10^{-2} mbar were collected and distilled through a Vigreux column. B.p.: 62 °C/17 mbar; yield: 4.93 g (38 mmol, 85%).

Catalytic epoxidation of cyclooctene with 1 mol% catalyst based on olefin: Molybdenum trioxide (Fluka, 260 mg, 1.80 mmol) was added to trisdodecylamine (Merck, 930 mg, 1.80 mmol), hydrogen peroxide (30%, 41.00 g, 360 mmol), and chloroform (20 mL). Within 20 min of stirring at 25 °C the organic phase became yellow. Cyclooctene (19.80 g, 180.0 mmol) was added to the biphasic catalyst system. After 4 h of stirring at 25 °C (85% conversion of olefin) a second portion of hydrogen peroxide (30%, 41.00 g, 360 mmol) was added and the mixture was stirred for another 16 h at 25 °C to achieve full conversion. The yellow organic layer was separated and washed with 4×40 mL water. Volatiles at 65 °C/10^{-2} mbar were collected and distilled through a Vigreux column. B.p.: 80 °C/17 mbar; yield: 22.15 g (175 mmol, 97%) white solid.

Acknowledgment

We gratefully acknowledge financial support from the Deutsche Forschungsgemeinschaft (Sonderforschungsbereich 347 „Selektive Reaktionen Metall-aktivierter Moleküle“ and Schwerpunktprogramm „Sauerstofftransfer/Peroxidchemie“) and from the Fonds der Chemischen Industrie (financial support and a generous fellowship to R.S). J.S. thanks the collaborators in BASF AG (J.-H. Teles, M. Schulz, and A. Walch) for stimulating discussions and for their support. Thanks are due to the Leibnitz-Rechenzentrum (München) and the Konrad-Zuse-Rechenzentrum (Berlin) for providing computation time on CRAY computers, and to P. Ruff (Rechenzentrum Würzburg) for helpful support.

[1] a) H. Mimoun, I. Seree de Roch, L. Sajus, *Bull. Soc. Chim. Fr.* **1969**, *5*, 1481 – 1492; b) H. Mimoun, I. Seree de Roch, L. Sajus, *Tetrahedron* **1970**, *26*, 37 – 49.

[2] a) A. D. Westland, F. Haque, J.-M. Bouchard, *Inorg. Chem.* **1980**, *19*, 2255 – 2259; b) W. Winter, C. Mark, V. Schurig, *Inorg. Chem.* **1980**, *19*, 2045 – 2048; b) V. Schurig, K. Hintzer, U. Leyrer, C. Mark, P. Pitchen, H. B. Kagan, *J. Organomet. Chem.* **1989**, *370*, 81 – 96.

[3] Review articles: a) G. Strukul, *Catalytic Oxidations with Hydrogen Peroxide as Oxidant*, Kluwer, Dordrecht, **1992**; b) R. A. Sheldon, J. K. Kochi, *Metal-Catalyzed Oxidation of Organic Compounds*, Plenum Press, New York, **1981;** c) H. Mimoun, *Angew. Chem.* **1982**, *94*, 750 – 766; *Angew. Chem. Int. Ed. Engl.* **1982**, *21*, 734; d) K. A. Jørgensen, B. Schiøtt, *Chem. Rev.* **1990**, *90*, 1483 – 1506; f) H. Mimoun, *Comprehensive Coordination Chemistry*, *Vol. 6*, Pergamon Press, New York, **1988**, pp. 317 – 410.

[4] O. Bortolini, F. Di Furia, G. Modena, R. Seraglia, *J. Org. Chem.* **1985**, *50*, 2688 – 2690.

[5] Key references: a) C. Venturello, E. Alneri, M. Ricci, *J. Org. Chem.* **1983**, *48*, 3831 – 3833; b) Y. Ishii, K. Yamawaki, T. Yoshida, T. Ura, M. Ogawa, *J. Org. Chem.* **1987**, *52*, 1868 – 1870; c) R. Neumann, A. M. Khenkin, *J. Org. Chem.* **1987**, *52*, 7577 – 7579; d) D. C. Duncan, R. C.

  0947-6539/99/0511-3250 $ 17.50+.50/0

Chambers, E. Hecht, C. L. Hill, *J. Am. Chem. Soc.* **1995**, *117*, 681–691; e) A. C. Dengel, W. P. Griffith, B. C. Parkin, *J. Chem. Soc. Dalton Trans.* **1993**, 2683–2688; f) L. Salles, C. Aubry, F. Robert, G. Chottard, R. Thouvenot, H. Ledon, J.-M. Brégeault, *New J. Chem.* **1993**, *17*, 367–375.

[6] a) W. P. Griffith, B. C. Parkin, A. J. P. White, D. J. Williams, *J. Chem. Soc. Chem. Commun.* **1995**, 2183–2184; b) R. Neumann, M. Cohen, *Angew. Chem.* **1997**, *109*, 1810–1812; *Angew. Chem. Int. Ed. Engl.* **1997**, *36*, 1738–1740; c) M. Bösing, A. Nöh, I. Loose, B. Krebs, *J. Am. Chem. Soc.* **1998**, *120*, 7252–7259.

[7] Selected key references: a) W. A. Herrmann, R. W. Fischer, W. Scherer, M. Rauch, *Angew. Chem.* **1993**, *105*, 1209–1212; *Angew. Chem. Int. Ed. Engl.* **1993**, *32*, 1157–1160; b) W. A. Herrmann, R. W. Fischer, M. U. Rauch, W. Scherer, *J. Mol. Catal.* **1994**, *86*, 243–266; c) W. A. Herrmann, D. W. Marz, W. Wagner, J. G. Kuchler, G. Weichselbaumer, R. W. Fischer (Hoechst AG), DE 3902357, **1989**; EP 901014399, **1990**; d) W. A. Herrmann, H. Ding, R. M. Kratzer, F. E. Kühn, J. J. Haider, R. W. Fischer, *J. Organomet. Chem.* **1997**, *549*, 319–322.

[8] a) A. Butler, M. J. Clague, G. E. Meister, *Chem. Rev.* **1994**, 94, 625–638; b) V. Conte, F. Di Furia, S. Moro, *J. Mol. Catal.* **1995**, *104*, 159–169; c) V. Conte, F. Di Furia, S. Moro, *J. Mol. Catal.* **1997**, *120*, 93–99.

[9] M. H. Dickman, M. T. Pope, *Chem. Rev.* **1994**, *94*, 569–584.

[10] W. R. Thiel, J. Eppinger, *Chem. Eur. J.* **1997**, *3*, 696–705.

[11] a) M. Schulz, J. H. Teles, J. Sundermeyer (BASF AG), DE-A 19533331, **1995**; b) M. Schulz, J. H. Teles, J. Sundermeyer, G. Wahl (BASF AG), WO 97/10054, **1997**.

[12] The electrophilic and nucleophilic behavior of oxenoids M(η^2-OOR) has been pointed out by Boche et al.: a) G. Boche, F. Bosold, J. C. W. Lohrenz, *Angew. Chem.* **1994**, *106*, 1228–1230; *Angew. Chem. Int. Ed. Engl.* **1994**, *33*, 1161–1163; b) G. Boche, K. Möbus, K. Harms, M. Marsch, *J. Am. Chem. Soc.* **1996**, *118*, 2770–2771; c) G. Boche, K. Möbus, K. Harms, J. C. W. Lohrenz, M. Marsch, *Chem. Eur. J.* **1996**, *2*, 604–607.

[13] L. M. Schwane, R. C. Thompson, *Inorg. Chem.* **1989**, *28*, 3938–3946.

[14] D. Kleinhenz, G. Wahl, unpublished results; A. Walch, BASF AG Ludwigshafen, personel communication.

[15] W. Adam, D. Golsch, J. Sundermeyer, G. Wahl, *Chem. Ber.* **1996**, *129*, 1177–1182.

[16] W. R. Thiel, T. Priermeier, T. Bog, *J. Chem. Soc. Chem. Commun.* **1995**, 1871–1872, and references therein.

[17] J.-M. le Carpentier, R. Schlupp, R. Weiss, *Acta Crystallogr. Sect B* **1972**, *28*, 1278–1288.

[18] C. Brink Shoemaker, D. P. Shoemaker, L. V. McAfee, C. W. DeKock, *Acta Crystallogr. Sect. C* **1985**, *41*, 347–350.

[19] W. Thiel, T. Priermeier, *Angew. Chem.* **1995**, *107*, 1870–1871; *Angew. Chem. Int. Ed. Engl.* **1995**, *34*, 1737–1738.

[20] Isoelectronically related anionic complexes with $OER_3 = [OSiPh_3]^-$ have been published recently and structurally characterized as monomers: J.-Y. Piquemal, S. Halut, J.-M. Brégeault, *Angew. Chem.* **1998**, *110*, 1149–1152; *Angew. Chem. Int. Ed. Engl.* **1998**, *37*, 1146–1149.

[21] F. A. Cotton, R. M. Wing, *Inorg. Chem.* **1965**, *4*, 867–873.

[22] W. A. Nugent, J. M. Mayer, *Metal–Ligand Multiple Bonds*, Wiley, New York, **1988**.

[23] W. P. Griffith, T. D. Wickins, *J. Chem. Soc. A* **1968**, 397–400.

[24] A. C. Dengel, W. P. Griffith, R. D. Powell, A. C. Skapski, *J. Chem. Soc. Dalton Trans.* **1987**, 991–995.

[25] C. Venturello, R. D'Alioisio, J. C. J. Bart, M. Ricci, *J. Mol. Catal.* **1985**, *32*, 107–110.

[26] N. J. Campbell, J. Flanagan, W. P. Griffith, A. C. Skapski, *Transition Met. Chem.* **1985**, *10*, 353–354.

[27] a) C. Aubry, G. Chottard, N. Platzer, J.-M. Brégeault, R. Thouvenot, F. Chauveau, C. Huet, H. Ledon, *Inorg. Chem.* **1991**, *30*, 4409–4415; b) L. Salles, J.-Y. Piquermal, R. Thouvenot, C. Minot, J.-M. Brégeault, *J. Mol. Catal. A* **1997**, *117*, 375–387; L. Salles, F. Robert, V. Semmer, Y. Jeannin, J.-M. Brégeault, *Bull. Soc. Chim. Fr.* **1996**, *133*, 319–328; L. Salles, C. Aubry, R. Thouvenot, F. Robert, C. Doremieux, G. Chottard, H. Ledon, Y. Jeannin, J.-M. Brégeault, *Inorg. Chem.* **1994**, *33*, 871–878.

[28] V. Deckert, W. Kiefer, *Appl. Spectrosc.* **1992**, *46*, 322–328.

[29] T. Ziegler, *Chem. Rev.* **1991**, *61*, 651.

[30] J. Andzelm in *Density Functional Methods in Chemistry* (Eds.: J. Labanowski, J. Andzelm), Springer, New York, **1991**, and references therein.

[31] J. Andzelm, E. Wimmer, D. R. Salahub in *The Challenge of d and f Electrons: Theory and Computations*, ACS Symposium Series No. 394, American Chemical Society, Washington DC, **1989**, p. 228, and references cited therein. DGAUSS is available as part of the UniChem software from Cray Research Inc., Eagan (MN).

[32] Provided by Professor Salahub (Montreal).

[33] P. Hohenberg, W. Kohn, *Phys. Rev. B* **1964**, *136*, 864.

[34] J. Andzelm, E. Radzio, D. R. Salahub, *J. Comput. Chem.* **1985**, *6*, 520.

[35] N. Godbout, D. R. Salahub, J. Andzelm, E. Wimmer, *Can. J. Chem.* **1992**, **70**, 560.

[36] H. B. Schlegel in *Ab Initio Methods in Quantum Chemistry*, (Ed.: K. P. Lawley), Wiley, New York, **1987**, p. 249, and references therein.

[37] SYBYL: Tripos Associates, 1699 St. Hanley Road, Suite 303, St. Louis (MO 63114).

[38] D. F. McIntosh, M. R. Peterson, QCPE 342, **1991**.

[39] H. C. Fleischhauer, *Ph.D. Thesis*, Universität Düsseldorf, Germany, **1991**.

[40] E. B. Wilson, Jr., J. C. Decius, P. Cross, *Molecular Vibrations*, Dover Publications, New York, **1980**.

[41] S. Franks, F. R. Hartley, D. J. A. McCaffrey, *J. Chem. Soc. Perkin Trans.* **1979**, 3029–3033.

[42] a) R. K. Robins, B. E. Christensen, *J. Org. Chem.* **1951**, *16*, 324–327; b) C. Stuebe, W. M. Le Suer, G. R. Norman, *J. Am. Chem. Soc.* **1955**, *77*, 3526–3529.

[43] R. N. Meals, *J. Org. Chem.* **1944**, *9*, 211–218.

[44] H. Werner, A. Hampp, K. Peters, E. M. Peters, L. Walz, H. G. von Schnering, *Z. Naturforsch. Teil B* **1990**, *45*, 1548–1558.

[45] P. Schwab, H. Werner, *J. Chem. Soc. Dalton Trans.* **1994**, 3415–3425.

[46] G. M. Sheldrick, *Acta Crystallogr. Sect. A* **1990**, *46*, 467.

[47] G. M. Sheldrick, SHELXL-93, Universität Göttingen, **1993**.

[48] G. M. Sheldrick, SHELXS-96, Universität Göttingen, **1996**.

[49] G. M. Sheldrick, SHELXL-96, Universität Göttingen, **1996**.

[50] E. Keller, SCHAKAL-92, Universität Freiburg, **1992**.